NPS ARCHIVE
1960
HUSSMANN, H.

CHARACTERISTICS OF NEUTRON WAVES IN A SUBCRITICAL ASSEMBLY

HARRY L. HUSSMANN

DUDLEY KNOX LIBRARY
NAVAL POSTGRADUATE SCHOOL
MONTEREY, CA 93943-5101

CHARACTERISTICS OF NEUTRON WAVES IN A SUBCRITICAL ASSEMBLY

by

Harry L. Hussmann, III

A Thesis Submitted to the
Graduate Faculty in Partial Fulfillment of
The Requirements for the Degree of
MASTER OF SCIENCE

Major Subject: Nuclear Engineering

TABLE OF CONTENTS

		Page
I.	INTRODUCTION	1
II.	REVIEW OF THE LITERATURE	3
III.	LIST OF SYMBOLS	5
IV.	THEORETICAL ANALYSIS	7
V.	EXPERIMENTAL EQUIPMENT	18
	A. Subcritical Assembly	18
	B. Oscillator Unit	21
	C. Electronic Equipment	26
VI.	EXPERIMENTAL PROCEDURE	34
	A. Analysis of Neutron Waves	34
	B. Typical Run	43
VII.	RESULTS	45
VIII.	CONCLUSIONS	62
IX.	LITERATURE CITED	63
X.	ACKNOWLEDGMENTS	64
XI.	APPENDIX A: TABLES OF DATA	65
XII.	APPENDIX B: PHASE ANGLE AND AMPLITUDE TABULATION	68
XIII.	APPENDIX C: EVALUATION OF NEUTRON FLUX COEFFICIENTS	70
XIV.	APPENDIX D: CALCULATION OF STANDARD DEVIATION	76

I. [illegible] 1

II. [illegible] 1

III. [illegible] 1

IV. [illegible] 7

V. [illegible] 11

A. [illegible] 12
B. [illegible] 21
C. [illegible] 28

VI. [illegible] 31

A. [illegible] 32
B. [illegible] 37

VII. [illegible] 47

VIII. [illegible] 52

IX. [illegible] 57

X. [illegible] 61

XI. [illegible] 64

XII. [illegible] 66

XIII. [illegible] 70

XIV. [illegible] 76

I. INTRODUCTION

If an oscillating source of neutrons is placed in a diffusing and reproducing medium, the flux distribution in the medium will be affected by this oscillation. If the period of oscillation is low in relation to the periods of the delayed neutrons, the neutron intensity in the assembly rises and falls as a whole, the basic stationary shape being maintained. As the frequency of oscillation increases, the nature of the neutron response changes from the overall fluctuation characteristic at low frequencies to a propagated and attenuated wave which emanates from the vicinity of the oscillator.

As the neutrons diffuse at a finite velocity, the wave phase differs at various locations throughout the medium. By an analysis of this phase shift and a determination of the wave amplitude, an evaluation of the characteristics of the medium can be made.

Murray (3) discusses the principal advantages of a subcritical assembly, namely relative low cost and safety. In addition, he discusses the use of steady sources in a subcritical assembly to determine either the materials buckling or the thermal diffusion length.

By utilizing a periodically varying source, one should be able to measure these quantities in very small assemblies simply by increasing the frequency of oscillation. A method

has been investigated to permit rapid measurements of the phase lag and the relative amplitude of the neutron wave within a natural uranium, graphite moderated subcritical assembly. The method is relatively free of dependence on data plots, and can be extended with moderately simple changes to other subcritical and critical reactors.

In addition, this experiment was concerned with an investigation of the characteristics of the neutron wave throughout the assembly and any possible conflict with the theory. The source terms were derived and the effects of the higher harmonics of the source term were investigated.

II. REVIEW OF THE LITERATURE

The use of the theory of neutron waves in the measurement of nuclear parameters was first suggested by Weinberg and Schweinler (8). In a 1948 paper, the characteristics of an oscillating absorber in a critical reactor were discussed. It was determined that the oscillations caused reactor-wide synchronized fluctuations of the flux at frequencies low in relation to the inverse period of the delayed neutrons. When the frequency was increased, definite waves were formed. By comparing the wave magnitude of a "standard" absorber with that of an unknown absorber, the absorption cross section of the unknown could be determined.

Weinberg and Wigner (9) derived the equations for wave motion due to a point source in an infinite diffusing or multiplying medium. Equations for the wave velocity, attenuation distance, and wave length were derived as functions of the oscillator frequency. In a manner analogous to Angstrom's cyclic method of measuring thermal conductivity, the formulas for the diffusion coefficient in a diffusive medium, and the material buckling of a multiplying medium are derived. It is shown that the characteristic lengths and velocities are dependent on the "prompt" material buckling, that is the buckling due to prompt neutrons only, and as a consequence, experiments for measuring the prompt buckling can be made in smaller systems than are required for ex-

ponential experiments, simply by making the source oscillate at high frequencies.

Campbell and Stelson (1) made relaxation time measurements of the fundamental mode of thermal neutrons leaking from a subcritical U^{235}, water solution. A square wave, pulsed neutron source was developed by impinging modulated high energy protons on a beryllium target, which in turn excited a uranyl fluoride solution. The volume of the assembly, hence the buckling, was varied and the half life of the neutrons determined over the appropriate range.

Kaievski in France has conducted some experimentation with neutron waves. With Horowitz (4), he determined the transport mean free path of thermal neutrons in heavy water.

In Sweden, Sjöstrand (5) has developed a method of determining prompt neutron decay time and the amount of reactivity by which a reactor is below criticality, using neutron waves. The waves were generated by the action of a modulated ion beam impinging on a Zr-T target. A (T,D) reaction caused the emission of 14 mev neutrons. The flux was measured by a BF_3 proportional counter feeding into a 40 channel time analyzer, permitting a study of the time variation of the neutron flux in the reactor.

III. LIST OF SYMBOLS

a	Extrapolated length of assembly	cm.
B^2	Buckling	$cm.^{-2}$
b	Extrapolated width of assembly	cm.
c	Extrapolated height of assembly	cm.
D	Thermal neutron diffusion coefficient	cm.
$k_{p\infty}$	Infinite multiplication factor	
N	Total counts	counts
n	Number of oscillations	cycles
R	Total counting rate	counts $min.^{-1}$
R_s	Steady component of counting rate	counts $min.^{-1}$
R_w	Counting rate of impressed sinusoidal wave	counts $min.^{-1}$
S	Time dependent source strength	neutrons $cm.^{-3} sec.^{-1}$
S_o	Steady state source strength	neutrons $cm.^{-3} sec.^{-1}$
S_t	Total source strength	neutrons $cm.^{-3} sec.^{-1}$
T	Time of travel	sec.
T'	Period of oscillator	sec.
t	Time	sec.
V_w	Wave propagation velocity	cm. $sec.^{-1}$
v	Neutron velocity	cm. $sec.^{-1}$
β^2	Complex material buckling	$cm.^{-2}$
γ	Steady component inverse relaxation length	$cm.^{-1}$
θ	Phase lag	radians

LIST OF SYMBOLS

ξ	Frequency dependent lag parameter	cm^{-1}
β_h	Wave inverse relaxation length	cm^{-1}
Σ_a	Thermal neutron absorption cross section	cm^{-1}
σ	Statistical standard deviation	
τ	Fermi age	cm^2
Φ	Time dependent amplitude of sinusoidal flux variation	neutrons $cm.^{-2}sec.^{-1}$
Φ_o	Steady component of thermal neutron flux	neutrons $cm.^{-2}sec.^{-1}$
ϕ	Total thermal flux	neutrons $cm.^{-2}sec.^{-1}$
ω	Oscillator angular frequency	radians $sec.^{-1}$

IV. THEORETICAL ANALYSIS

An analysis of neutron wave propagation has been developed by Uhrig[1]. If a sinuscidal source of neutrons is utilized in a subcritical assembly, the variation of the flux throughout the assembly will be sinusoidal. For low frequencies, the flux throughout the assembly varies in phase with the source strength variation. As the frequency of variation of source strength increases, the flux continues to vary with the period of the oscillating source, but due to the finite time required for the neutrons to travel up the assembly, a definite phase lag develops. At very high frequencies, this lag may amount to several cycles. By analysis of this variation of phase and the attenuation of the wave with vertical position, the characteristics of the waves and the assembly can be determined.

Consider a source of strength

$$S_t = S_o + Se^{i\omega t} \qquad (1)$$

placed at the base of a subcritical assembly. As a negative source strength is impossible, S_o must of necessity be greater than S. Throughout the medium, the flux will have the same

---

[1]Uhrig, R. E., Ames, Iowa. Neutron waves in a subcritical assembly. Private communication. 1959.

---

[1]Gordon D. Ely Jones, Jones Junction County Jr & Sup-
ertime Company, Private communication, 1977.

time dependence as the source, and if the multiplication of the assembly is not too large, the flux may be written as

$$\phi(r,t) = \Phi_o(r) + \Phi(r)\, e^{i\omega t} \qquad (2)$$

which implies that the variables of space and time are separable.

If a volume is selected in a region where most of the neutrons have been produced by fission, the non equilibrium diffusion equation for thermal neutrons can be used

$$D\nabla^2\phi - \Sigma_a \phi + k_{p\infty} \Sigma_a e^{-B_g^2\tau} \phi = \frac{1}{v} \frac{\partial \phi}{\partial t} \qquad (3)$$

where $D\nabla^2\phi$ is the net diffusion into the given volume, $\Sigma_a \phi$ is the number of neutrons absorbed in the volume per unit time, $k_{p\infty}\, e^{-B_g^2\tau} \phi$ is the integrally generated fission neutrons and the term $\frac{1}{v} \frac{\partial \phi}{\partial t}$ corresponds to the net population change of neutrons per unit volume per unit time. The source term is given in Glasstone and Edlund (2), and is composed of the prompt multiplication factor, $k_{p\infty}$, used because the period of oscillation is small compared to the lifetime of the delayed neutrons, $\Sigma_a \phi$, the absorption by fission material per unit time, and the exponential term $e^{-B_g^2\tau}$ to account for leakage during the thermalizing period. The volume element investigated is selected away from the source, and source neutrons are considered to be introduced into the system only as a result of fission phenomena.

Substitution of Equation 2 into Equation 3 yields

$$D\nabla^2 \Phi_o + D\nabla^2 \Phi e^{i\omega t} - \Sigma_a \Phi_o - \Sigma_a \Phi e^{i\omega t} + k_{p\infty}\Sigma_a e^{-B_g^2\tau}\Phi_o + k_{p\infty}\Sigma_a \Phi e^{-B_g^2\tau} e^{i\omega t} = \frac{i\omega}{v}\Phi e^{i\omega t} \qquad (4)$$

The steady state portion of the flux may be separated out as

$$D\nabla^2 \Phi_o - \Sigma_a \Phi_o + k_{p\infty}\Sigma_a e^{-B^2\tau}\Phi_o = 0 \qquad (5)$$

If the static material buckling is defined by

$$B_m^2 = \frac{\Sigma_a}{D}\left[k_{p\infty} e^{-B^2\tau} - 1\right] \qquad (6)$$

Equation 5 reduces to

$$\nabla^2 \Phi_o + B_m^2 \Phi_o = 0 \qquad (7)$$

As the assembly is a rectangular parallelepiped, cartesian coordinates are selected, and Equation 7 becomes

$$\frac{\partial^2 \Phi_o}{\partial x^2} + \frac{\partial^2 \Phi_o}{\partial y^2} + \frac{\partial^2 \Phi_o}{\partial z^2} + B_m^2 \Phi_o = 0 \qquad (8)$$

It is assumed that Φ_o can be expressed as independent functions of the three coordinates chosen, or

$$\Phi_o = X(x)\, Y(y)\, Z(z) \qquad (9)$$

Substitution of Equation 9 into Equation 8, and dividing all terms by X(x) Y(y) Z(z), yields

$$\frac{1}{X(x)} \frac{\partial^2 X(x)}{\partial x^2} + \frac{1}{Y(y)} \frac{\partial^2 Y(y)}{\partial y^2} + \frac{1}{Z(z)} \frac{\partial^2 Z(z)}{\partial z^2}$$

$$+ B_m^2 = 0 \qquad (10)$$

Since each term of Equation 10 is a function of one variable only, it can only be satisfied if each term is equal to a constant. If these constants are selected equal to $-\alpha^2$, $-\beta^2$, and γ^2, Equation 10 becomes

$$-\alpha^2 - \beta^2 + \gamma^2 + B_m^2 = 0 \qquad (11)$$

where

$$-\alpha^2 = \frac{1}{X(x)} \frac{\partial^2 X(x)}{\partial x^2}$$

$$-\beta^2 = \frac{1}{Y(y)} \frac{\partial^2 Y(y)}{\partial y^2}$$

$$\gamma^2 = \frac{1}{Z(z)} \frac{\partial^2 Z(z)}{\partial z^2}$$

The solution to Equation 10 becomes

$$X(x) = A_1 \cos \alpha x + C_1 \sin \alpha x \qquad (12)$$

$$Y(y) = A_2 \cos \beta y + C_2 \sin \beta y$$

$$Z(z) = A_3 \, e^{-\gamma z} + C_3 \, e^{\gamma z}$$

The boundary conditions stipulate that the flux will vanish at the extrapolated boundaries, or

$$\Phi_o(a/2,y,z) = \Phi_o(x,b/2,z) = \Phi_o(x,y,c) = 0 \qquad (13)$$

Utilizing this information, the three components of steady

state flux are

$$X(x) = A_1 \cos \frac{m\pi x}{a} \qquad m = 1, 3, 5, \ldots$$

$$Y(y) = A_2 \cos \frac{n\pi y}{b} \qquad n = 1, 3, 5, \ldots$$

$$Z(z) = A_3 e^{-\gamma z} \left[1 - e^{-2\gamma z(c - z)}\right] \tag{14}$$

If values of z near the top are excluded, the end correction factor in the square brackets is approximately one. As there are an infinite number of odd integer values for m and n, the general solution for the flux is a linear summation of all possible solutions

$$\Phi_o(x,y,z) = \sum_{m=1}^{\infty} \sum_{n=1}^{\infty} A_{mn} \cos \frac{m\pi x}{a} \cos \frac{n\pi y}{b} e^{-\gamma_{mn} z} \tag{15}$$

It is to be seen in Equation 15 that γ_{mn} is the inverse relaxation length of the mn mode in the z direction. This is the same inverse relaxation length that would be characteristic of a subcritical assembly with a steady source. The solution for Φ_o shows that

$$\alpha = \frac{m\pi}{a} \tag{16}$$

$$\beta = \frac{n\pi}{b}$$

Substitution of Equation 16 into Equation 11 yields the value of this inverse relaxation length

$$\gamma_{mn}^2 = \left(\frac{m\pi}{a}\right)^2 + \left(\frac{n\pi}{b}\right)^2 - B_m^2 \tag{17}$$

In order to analyze the time dependent portion of the flux

in the assembly, the steady state component, Equation 5, is subtracted from the diffusion equation, Equation 4, to give

$$D\nabla^2\Phi\, e^{i\omega t} - \Sigma_a \Phi e^{i\omega t} + k_{p\infty}\Sigma_a \Phi e^{-B^2\tau}\, e^{i\omega t} = \frac{i\omega}{v}\Phi e^{i\omega t} \tag{18}$$

If Equation 18 is divided through by $De^{i\omega t}$, the resulting equation is

$$\nabla^2\Phi + \Phi\left[-\frac{\Sigma_a}{D} + \frac{k_{p\infty}\Sigma_a\, e^{-B^2\tau}}{D} - \frac{i\omega}{vD}\right] = 0 \tag{19}$$

or, if the complex material buckling is defined as

$$\beta_m^2 = \frac{\Sigma_a}{D}\left(k_{p\infty}\, e^{-B^2\tau} - 1\right) - i\left(\frac{\omega}{vD}\right) \tag{20}$$

the time dependent flux equation becomes

$$\nabla^2\Phi + \beta_m^2\Phi = 0 \tag{21}$$

It is of interest to note that the complex material buckling is composed of the static material buckling and an imaginary frequency dependent term. Substitution of Equation 6 into Equation 20 yields

$$\beta_m^2 = B_m^2 - i\frac{\omega}{vD} \tag{22}$$

The solution of Equation 21 is identical in form to the solution of the steady state equation, Equation 7, if the same boundary conditions are imposed. The general solution is

$$\Phi = \sum_{m=1}^{\infty} \sum_{n=1}^{\infty} C_{mn} \cos \frac{m\pi x}{a} \cos \frac{n\pi y}{b} e^{-\rho_{mn} z} \tag{23}$$

Here, ρ_{mn} is the inverse relaxation length for the mn mode of the time dependent portion of the flux, and is given by

$$\rho_{mn}^2 = \left(\frac{m\pi}{a}\right)^2 + \left(\frac{n\pi}{b}\right)^2 - \beta_m^2 \tag{24}$$

Substitution of Equation 15 and Equation 23 into Equation 2 gives the solution for the neutron flux as a function of space and time

$$\phi = \sum_{m=1}^{\infty} \sum_{n=1}^{\infty} \cos \frac{m\pi x}{a} \cos \frac{n\pi y}{b} \left[A_{mn} e^{-\gamma_{mn} z} + C_{mn} e^{i\omega t - \rho_{mn} z} \right] \tag{25}$$

For an evaluation of the constants, A_{mn} and C_{mn}, see Appendix C.

If β_{mn}^2 of Equation 22 is substituted into Equation 24, it can be seen that the complex inverse relaxation length is

$$\rho_{mn}^2 = \left(\frac{m\pi}{a}\right)^2 + \left(\frac{n\pi}{b}\right)^2 - B_m^2 + i \frac{\omega}{vD} \tag{26}$$

If Equation 17 and 26 are compared, the steady state inverse relaxation length can be related to the complex inverse relaxation length

$$\rho_{mn}^2 = \gamma_{mn}^2 + i \frac{\omega}{vD} \tag{27}$$

If a quantity ψ_{mn} is defined as

$$\psi_{mn}^2 = \left[\gamma_{mn}^4 + \left(\frac{\omega}{vD}\right)^2 \right]^{\frac{1}{2}} \tag{28}$$

the value of ρ_{mn} is found to be

$$\rho_{mn} = \left(\frac{\psi_{mn}^2 + \gamma_{mn}^2}{2} \right)^{\frac{1}{2}} + i \left(\frac{\psi_{mn}^2 - \gamma_{mn}^2}{2} \right)^{\frac{1}{2}} \tag{29}$$

Substitution of Equation 29 into Equation 25 gives

$$\phi = \sum_{m=1}^{\infty} \sum_{n=1}^{\infty} \cos \frac{m\pi x}{a} \cos \frac{n\pi y}{b} \left[A_{mn} e^{-\gamma_{mn} z} + C_{mn} \exp. \left\{ -\left(\frac{\psi_{mn}^2 + \gamma_{mn}^2}{2} \right)^{\frac{1}{2}} z + i \left(\omega t - \left\{ \left[\frac{\psi_{mn}^2 - \gamma_{mn}^2}{2} \right]^{\frac{1}{2}} z \right) \right\} \right]$$

$$m = 1, 3, 5, \ldots$$

$$n = 1, 3, 5, \ldots \tag{30}$$

The steady state component is represented in the brackets by the term $e^{-\gamma_{mn} z}$. It can be seen that this steady state component is attenuated in the z direction with an inverse relaxation length of γ_{mn}. The remainder of the bracketed term is associated with the attenuation of the time varying flux, and is of the form

$$e^{-\rho_R z + i(\omega t - \xi z)}$$

where the parameters ρ_R and ξ will be defined later. This type of function can also be expressed as

$$e^{-\rho_R z} \left[\cos(\omega t - \xi z) + i \sin (\omega t - \xi z) \right]$$

which can be analyzed as a periodic sinusoidal function having amplitude of $e^{-\rho_R z}$, a wave form of frequency ω, and a lag angle of ξz. The component $\rho_R z$ is a measure of the amplitude, and the factor ρ_R is the inverse relaxation length associated with the wave.

$$\rho_{R_{mn}} = \left[\frac{\psi_{mn}^2 + \gamma_{mn}^2}{2}\right]^{\frac{1}{2}} \tag{31}$$

The wave is produced at a frequency ω by the oscillator, but due to the distance it must travel from the source to a point z, there is a lag encountered equivalent to ξz. The time T for the wave to travel from the source to the point z, is equal to the distance divided by the wave velocity, or

$$T = \frac{z}{V_w} \tag{32}$$

From this analogy, and utilizing Equation 30, the time T is

$$T = \frac{z}{\omega}\left[\frac{\psi_{mn}^2 - \gamma_{mn}^2}{2}\right]^{\frac{1}{2}} \tag{33}$$

To find the wave velocity, equate Equations 32 and 33

$$V_w = \omega\left[\frac{2}{\psi_{mn}^2 - \gamma_{mn}}\right]^{\frac{1}{2}} \tag{34}$$

The phase angle Θ of the neutron wave is related to the neutron wave velocity by

$$T = \frac{z}{V_w} = \frac{\Theta}{\omega} \tag{35}$$

Combination of Equation 34 with Equation 35 gives

$$\theta = \left[\frac{\psi_{mn}^2 - \gamma_{mn}^2}{2}\right]^{\frac{1}{2}} z = \xi_\gamma z \qquad (36)$$

where ξ_γ is the frequency dependent constant of proportionality.

The real component of the inverse relaxation length, ρ_R can be determined from a semi-logarithmic plot of the neutron wave amplitude, Φ versus z.

Substitution of Equations 17 and 28 into Equation 31 and rearranging gives a value of the material buckling as follows

$$B_m^2 = \left[\frac{\pi}{a}\right]^2 + \left[\frac{\pi}{b}\right]^2 + \left[\frac{\omega}{2vD\rho_R}\right]^2 - \rho_R^2 \qquad (37)$$

Inspection of Equation 36 indicates that the value ξ_γ would equal the slope of a linear plot of θ versus z, or

$$\xi_\gamma = \frac{\Delta\theta}{\Delta z} = \left[\frac{\psi^2 - \gamma^2}{2}\right]^{\frac{1}{2}} \qquad (38)$$

Substitution of Equations 17 and 28 into Equation 38, and rearranging gives

$$B_m^2 = \left[\frac{\pi}{a}\right]^2 + \left[\frac{\pi}{b}\right]^2 + \xi_\gamma^2 - \left[\frac{\omega}{2vD\xi_\gamma}\right]^2 \qquad (39)$$

Comparison of Equation 37 and Equation 39 shows

$$\rho_R^2 - \left[\frac{\omega}{2vD\rho_R}\right]^2 = -\xi_\gamma^2 + \left[\frac{\omega}{2vD\xi_\gamma}\right]^2 \qquad (40)$$

which can be solved for the diffusion coefficient D

$$D = \frac{\omega}{2v\xi_\gamma\rho_R} \qquad (41)$$

Substitution of this value of D into Equation 37 or Equation 39 gives a value for the buckling

$$B_m^2 = \left(\frac{\pi}{a}\right)^2 + \left(\frac{\pi}{b}\right)^2 + \xi^2 - \rho_R^2 \qquad (42)$$

The subscripts mn have been dropped in the equations for the material buckling as the definition of material buckling specifically applies to the m = n = 1 mode.

It is apparent from Equation 42 that the materials buckling can be found if the values of ξ and ρ_R and the physical dimensions of the assembly are known. With these values known, plus the frequency of oscillation and the neutron thermal velocity, the diffusion coefficient can be found from Equation 41.

V. EXPERIMENTAL EQUIPMENT

A. Subcritical Assembly

The graphite moderated subcritical assembly of the Iowa State University was utilized in this experiment. The east face of the assembly which is shown in Figure 1 consists of fourteen layers of AGR grade blocks, the lower nine layers measuring 6" x 6" x 62" while the upper layers were 5" x 6" x 62" blocks. The "extrapolation length" of the assembly has been calculated as 0.75 inches (6). The assembly was covered on the top and sides by a 0.010 inch sheet of cadmium sandwiched between a plywood-masonite retaining wall. This cadmium produced an effective "black wall" for thermal neutrons. The distance between the cadmium sheets in the north-south direction was 60.5 inches; in the east-west direction, 62.5 inches, giving an effective size of 62.0 by 64.0 inches. The height of the graphite in the assembly was 79.0 inches.

Each block of the assembly had rounded corners so that when stacked together, the corners formed a channel with the cross section of a four cusped hypocycloid. For identification purposes, the channels investigated were assigned numbers. Twenty-five channels were available consisting of rows at 12", 24", 36", 48", and 59" above the graphite base. These rows were numbered 1, 2, 3, 4, and 5 respectively. The channels were also aligned vertically, with columns on the

Figure 1. Subcritical assembly

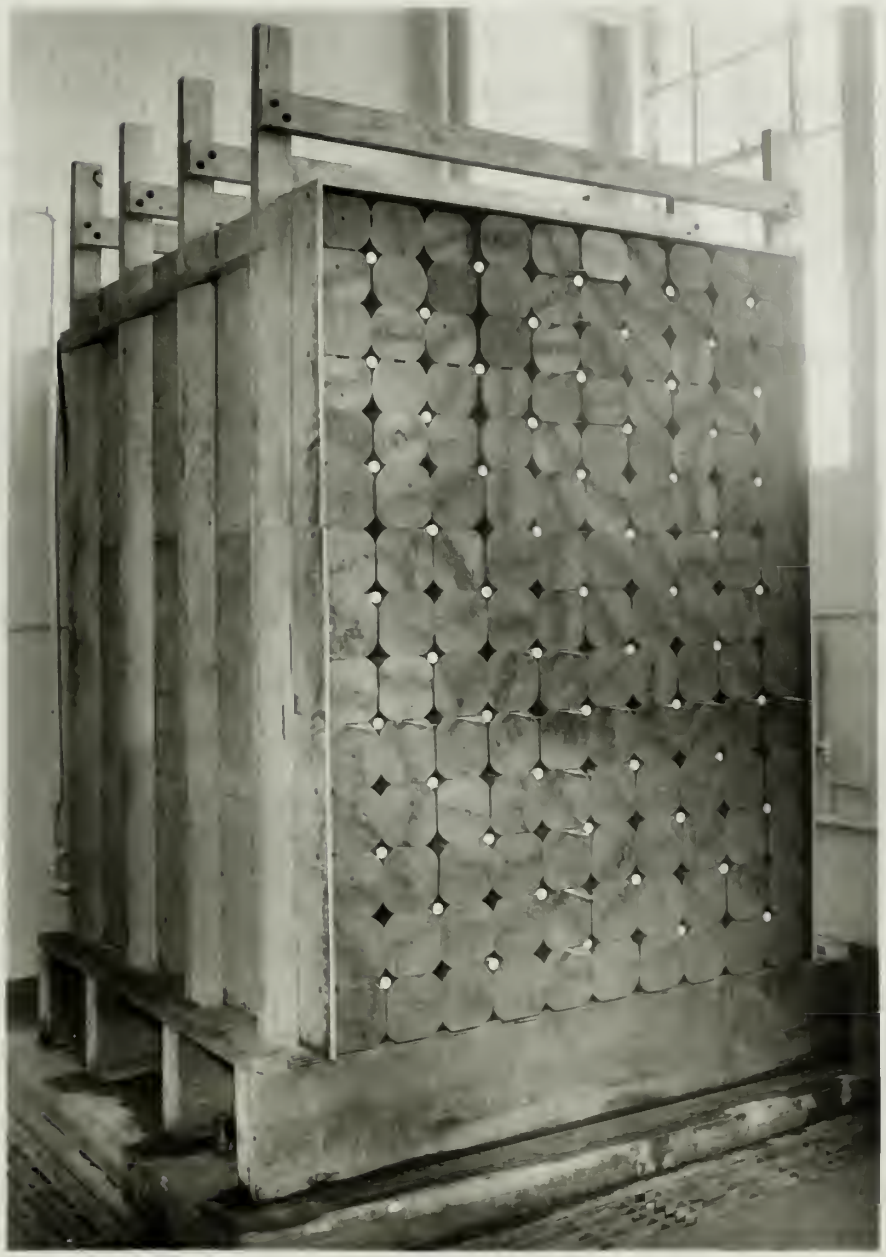

centerline of the assembly, and at points 12" and 24" to the north and south of the centerline. These columns were lettered from south to north as columns a, b, c, d, and e respectively. Thus, the channel six inches from the south wall and four feet up is channel 4a.

For this experiment, natural uranium slugs were placed in alternating channels to form a square lattice of approximately 8.5 inches per side. The slugs were cylindrical in shape, 1.00 inches in diameter and 8.00 inches long. Seven slugs were inserted into each of the channels utilized.

The assembly was supported on a pedestal consisting of 4 x 12 inch planks arranged so as to provide three void spaces beneath the assembly. Into the outer two voids were placed two water tanks which provided both personnel protection from the neutron source and moderation of the source neutrons. Into the center void was placed the oscillator assembly.

In summary, the effective dimensions of the assembly are 62" x 64" x 79.8". The value of static material buckling utilized for the theoretical calculations was $B_m^2 = 0.000374 \pm 0.000055$ in^{-2} (7), while the theoretical diffusion coefficient used was D = 0.9 cm. (9).

B. Oscillator Unit

The oscillator and photocell unit is pictured in Figure 2. When in operation, it is inserted into the void shown

Figure 2. Oscillator unit

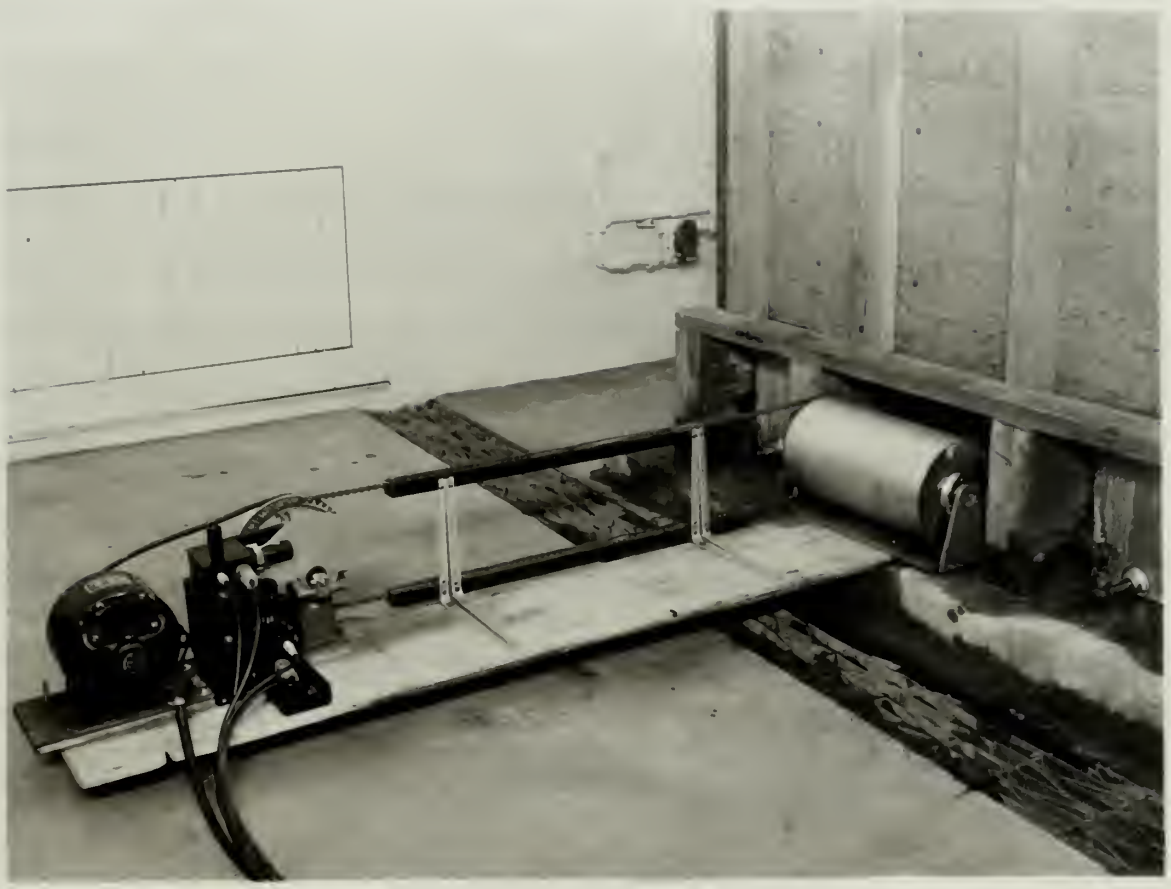

until the oscillator is immediately below the assembly centerline.

A schematic of the oscillator is shown in Figure 3. The source consisted of five cylindrical one-curie plutonium-beryllium sources, one inch in diameter and one and three-eighths inches long. These sources were placed in the axle (source retainer) of the oscillator unit which was constrained so as not to rotate. Around the axle was built up an aluminum cylinder of 7 3/8 inch diameter filled with paraffin and also immobile. It was desired to restrict neutron escape from the oscillator, so that the neutrons came out only in a horizontal direction. The purpose of this restriction was to combat a directional tendency that had previously been noted, and which effectively altered the concept of a point source. To control this tendency, 0.020" cadmium sheet metal was cemented to the top and bottom 90° of the stationery cylinder.

Outside of this cylinder was a 7 3/4 inch aluminum cylinder which was free to rotate about the common axis. On the inside of this cylinder was cemented a 0.030 inch thick cadmium pattern consisting of two sine cycles. The rotation of this cylinder permitted a sinuscidal variation of neutron flux to enter the assembly. Rigidly attached to one base of the patterned cylinder was a bicycle sprocket. A bicycle type chain was used to drive the sprocket and attached pat-

world the qualities to immediately bring the personality evaluation.

A refinement of the multiview is shown in figure 3. The picture presented of five stylistic manifestations, each built in diversity and representative quality. These particular forms pictured in the auto industry (picture courtesy of the Automotive Golf Cloth) are available on as not to repeat. Should the auto use build up an element collapse of 3 3/4 load capacity (Cloth used personality and also possibly. It may possess to buildup another answer than the multiview, in that the question used only in a particular diversion. The purpose of this presentation that is evaluate a diversified sentence that may personally been noted and think extensively picture the answer of a right matter. In another auto business, Chrysler national about sales economic is the only one matter for of the existing options.

Details of this multiple use a 3 3/4 load element stylistic quality use time to notify where the common auto. In the basics of this question the rounded a fully load three session pattern consisting of the five choices. The question of this multiple purpose a standard visitors of feature time to enjoy the personality. Finally attached to the loss of the personal opinion use a lightly approach. A pattern life depict use used to study the personal expression.

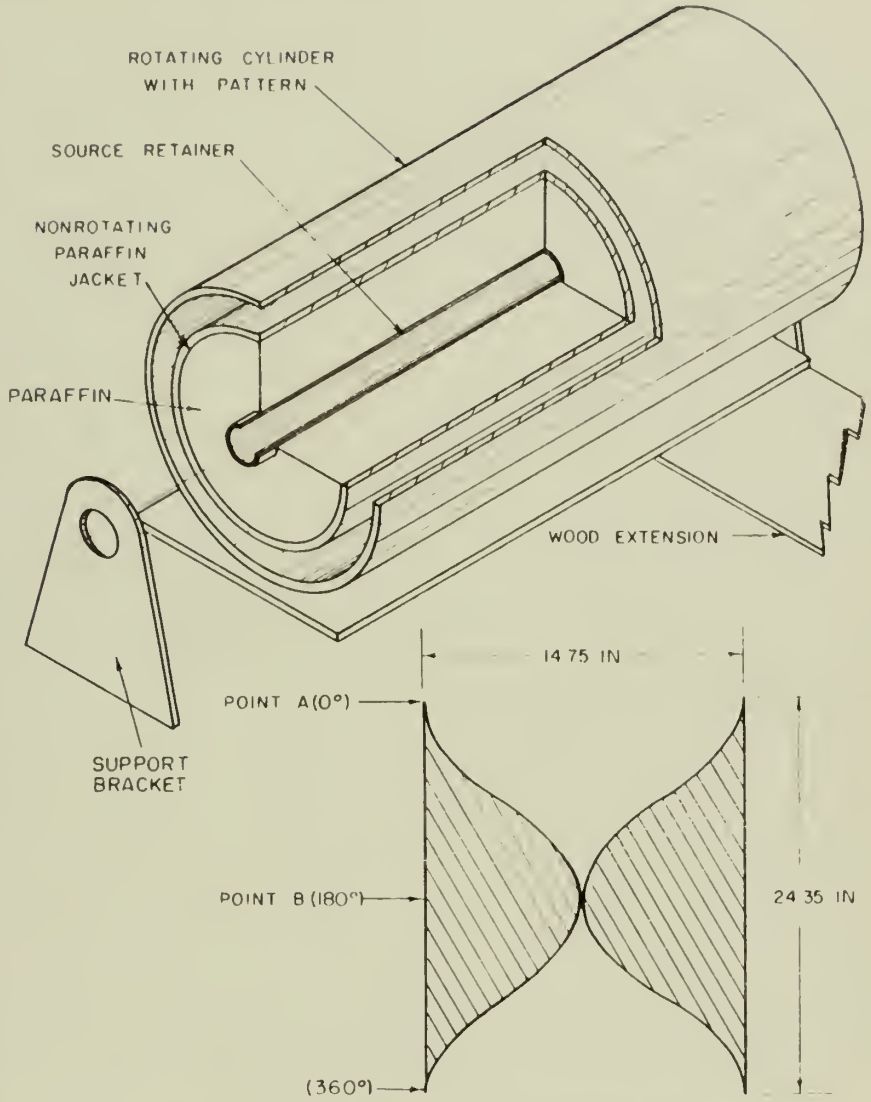

Figure 3. Oscillator unit and cadmium pattern detail

terned cylinder from another sprocket outside the subcritical assembly. This sprocket in turn was belt driven by a constant speed one-sixth horsepower AC motor rated at 1725 revolutions per minute.

On the same shaft with the outside sprocket was the light chopper, or synchronized timer, which consisted of a disc of seven inch diameter. This disc was machined so that the two alternate 90° sectors were cut away. The chopper rotated so as to cut the light beam between a small pre-focused bulb and its associated photocell. This served as a triggering unit to cause one of two scalars to count. By counting for a ninety degree sector on the chopper, 180° of the sinusoidal cycle was counted.

Two photocell units were utilized, placed 45° apart in relation to the chopper. Each photocell unit controlled two scalars, one to count when the light beam was unimpeded, and the other scalar to count when the beam was interrupted by the chopper blade. By this arrangement, each scalar counted for 180° of oscillator rotation, but each scalar counted a different period of the cycle.

C. Electronic Equipment

In order to obtain precise measurements of the neutron flux during specified portions of the oscillator cycle, a rather elaborate switching arrangement was devised.

A schematic of the overall arrangement of equipment is shown in Figure 4. Rigidly attached to the chain drive axle was the seven inch circular disc, having alternate 90° sectors cut out. This synchronized timer disc was aligned so as to cut the light beams (Light #1 only shown in the figure) at 0°, 90°, 180°, and 270° of drum rotation. The light beam, consisting of a prefocused flashlight bulb, General Electric Type 222, was focused onto a hole pierced into the hood over a phototube. When light impinged on the hole, the phototube conducted a current which was fed into a cathode follower amplifier tube and circuit. The output of the cathode follower was fed into the coincidence-anticoincidence circuit. The light, cathode follower, coincidence-anticoincidence circuit, and two of the slave scalars are repeated identically for light number two and its associated equipment. Only one of these circuits will be discussed.

It is worthwhile now to observe the other branch of the electronic circuitry, starting with the neutron detector, a BF_3 tube, manufactured by the N. Wood Counter Laboratory. This tube was one inch in diameter with a six inch shank and exhibited a voltage plateau at 2325 volts.

The pulses from this tube were fed into the master scalar, a Nuclear-Chicago Model 186 scalar operated at a sensitivity of 5 millivolts. This master scalar registered the total counts noted by the BF_3 tube.

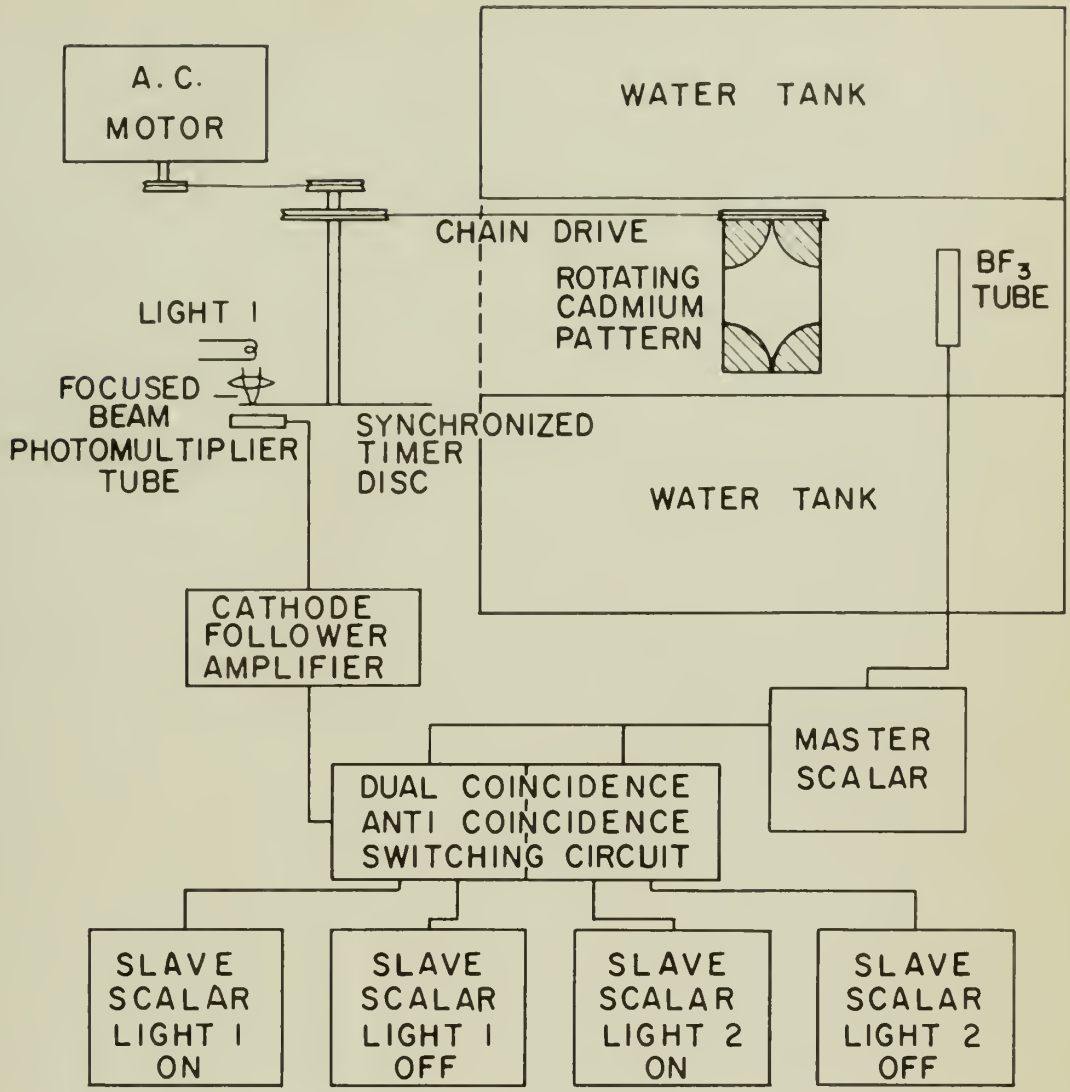

Figure 4. Schematic of associated equipment

From the rate-meter jack in the rear of the master scalar, a 5 volt (negative) square pulse, 5 microseconds wide, was fed into the coincidence-anticoincidence circuit. All counts registered by the master scalar were fed into this coincidence circuit. The function of this circuit was to route the counts to the proper slave scalar during any given time interval.

The circuit diagram of the coincidence-anticoincidence switching circuit is shown in Figure 5. Basically, it consists of a power source, twin cathode follower circuits and twin switching (coincidence-anticoincidence) circuits. When the light from the flashlight bulb is unimpeded, the phototube (929) conducts, impressing a signal on the grid of the cathode follower tube (6C4). This signal is amplified and sent to the coincidence-anticoincidence circuit. It is to be noted that the signal out of the cathode follower is of negative voltage in relation to ground.

As both circuits are identical, only circuit one will be discussed. The signal is fed to one grid of V1 and to both grids of V3. Tube V3 is utilized as a cathode follower tube and effectively impedes current flow when its grids are forced negative. The result is that no signal is evidenced at the "Output to 'off' Scalar #1" connection when a signal (i.e., light on) comes from the cathode follower.

Without a signal impressed (i.e., light off), the left

Figure 5. Circuit diagram, coincidence anticoircidence circuit

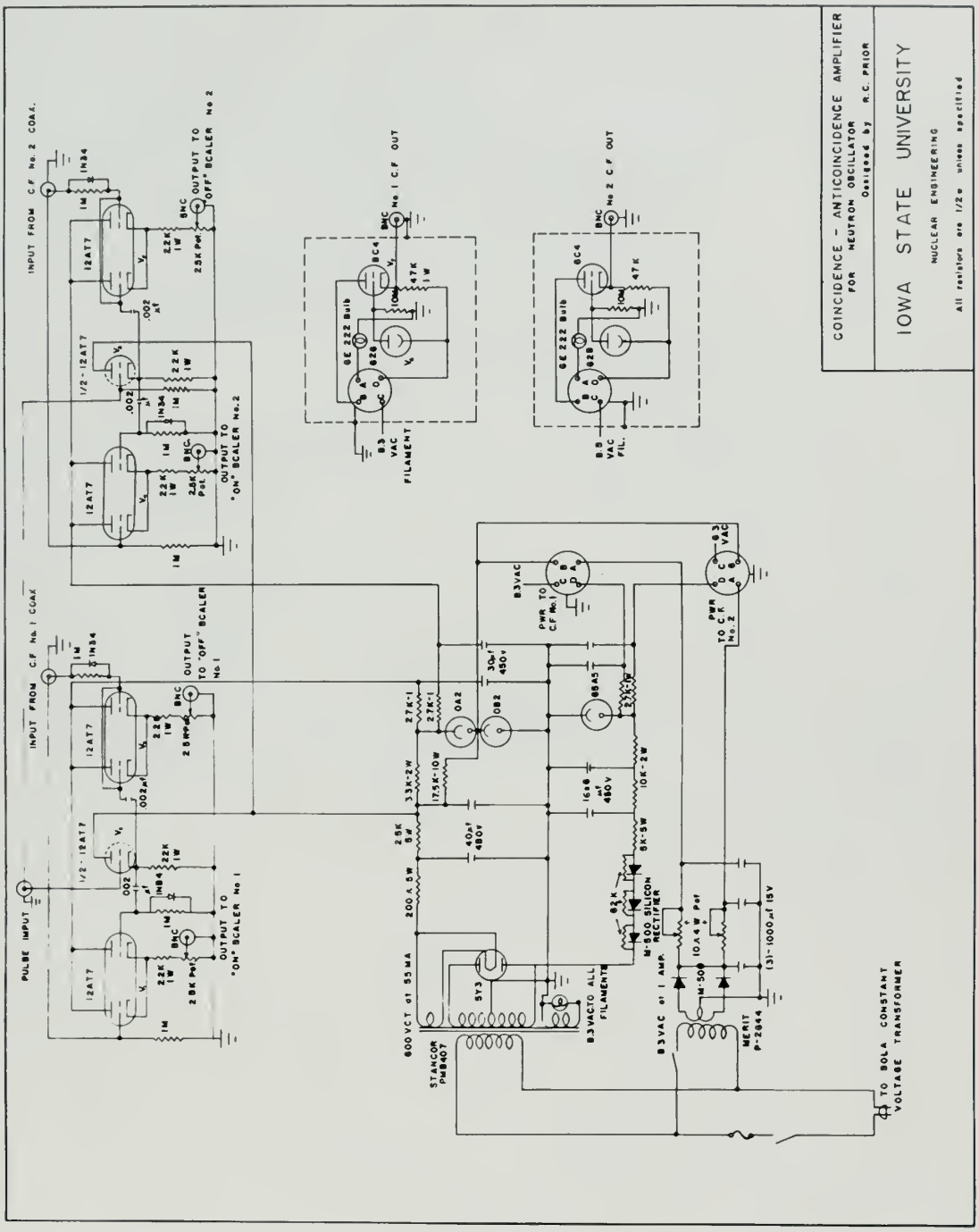
COINCIDENCE - ANTICOINCIDENCE AMPLIFIER
FOR NEUTRON OSCILLATOR
Designed by R.C. PRIOR
IOWA STATE UNIVERSITY
NUCLEAR ENGINEERING
All resistors are 1/2w unless specified
INPUT FROM C.F. No. 2 COAX.
INPUT FROM C.F. No. 1 COAX.
PULSE INPUT
OUTPUT TO "OFF" SCALER No. 2
OUTPUT TO "ON" SCALER No. 2
OUTPUT TO "OFF" SCALER No. 1
OUTPUT TO "ON" SCALER No. 1
No. 1 C.F. OUT
No. 2 C.F. OUT
GE 222 Bulb
B3 VAC FILAMENT
B3 VAC FIL.
PWR TO C.F. No. 1
PWR TO C.F. No. 2
B3 VAC
B3 VAC
600 VCT at 55 MA
STANCOR PM8407
5Y3
B3 VAC TO ALL FILAMENTS
B3 VAC at 1 AMP
W-800 SILICON RECTIFIER
W-500
MERIT P-2844
TO BOLA CONSTANT VOLTAGE TRANSFORMER

grid of V1 is at a slight positive potential and passes the only current that flows through the tube. This causes the right circuit of V1 to be non conducting, and the pulse output of V2 is not evidenced as a voltage change across the "Output to 'on' Scalar #1".

When the input signal from the cathode follower is impressed on the left grid of tube V1, this loop ceases conducting, and the right grid circuit conducts, in effect closing the circuit of the right grid. Now, when a pulse input is fed to V2, the voltage change is evidenced as a voltage drop across the output resistor, and this signal is fed as a pulse to the 'on' scalar.

In summary, the pulses from the master scalar are impressed across both of the cathode resistors of tubes V1 and V3. When a negative signal (light on) is fed in, V3 becomes non-conducting and the pulse is not evidenced as a voltage drop in the cathode resistor of V3. The same negative signal in V1 causes the left grid circuit to become non-conducting while the right circuit takes the entire current flow. This effectively closes the circuit of the right grid and the pulse input of the master scalar is fed out to the slave 'on' scalar.

The 'light on' slave scalar used for this experiment was a Nuclear Chicago Model 192 Ultrascalar, while the 'light off' scalar was a Baird-Atomic unit consisting of

a Model 134 scalar, Model 630 timer, and Model 212 Amplifier.

VI. EXPERIMENTAL PROCEDURE

A. Analysis of Neutron Waves

In the determination of the characteristics of a subcritical assembly using neutron waves, it is necessary to determine the phase of the wave and the amplitude of the wave at a given point. If these values are known, it is possible to determine wave velocity and attenuation length of the wave, and the characteristics of the subcritical assembly itself. One of the purposes of this experiment was to devise a satisfactory method of determining this phase and amplitude; and, having the method, to determine the correlation between theory and experiment.

It was particularly desirable that the waves be studied at as high a frequency of oscillation as possible. At high frequencies, on the order of 100 radians per second or greater, the wave velocity, phase shift, and inverse attenuation length increase significantly, permitting more accurate determinations of the assembly characteristics using a shorter period of time and a smaller portion of the assembly. The magnitude of these changes is illustrated graphically in Figures 6, 7, and 8. The value ξ is a measure of the wave phase change within the assembly, while ρ_R can be considered as the inverse relaxation length of the wave amplitude. It is to be realized that the inverse relaxation

4. Analysis of Surface Data

In the determination of the thermodynamic properties of a hydrodynamic boundary value problem, it is necessary to determine the change of the state of the water as a given point. If these values are known, it is possible to determine many relative properties of the problem. Some of the properties of this boundary value problem are determined by the mathematical theory and experiment.

It was previously mentioned that the waves be studied in this a frequency of oscillation as period". At high frequencies, or the order of 100 radians per second or greater, the wave velocity, phase velocity, and Lagrange displacement are approximately zero. Therefore, the displacements of the boundary particles are a function of the initial position of time and a positive position of the boundary. The equations of these waves is differential equations in φ, and η. The value ξ is a function of the wave phase velocity which is constant, while η can be considered as the Lagrange displacement length of the free surface. If ξ is to be evaluated

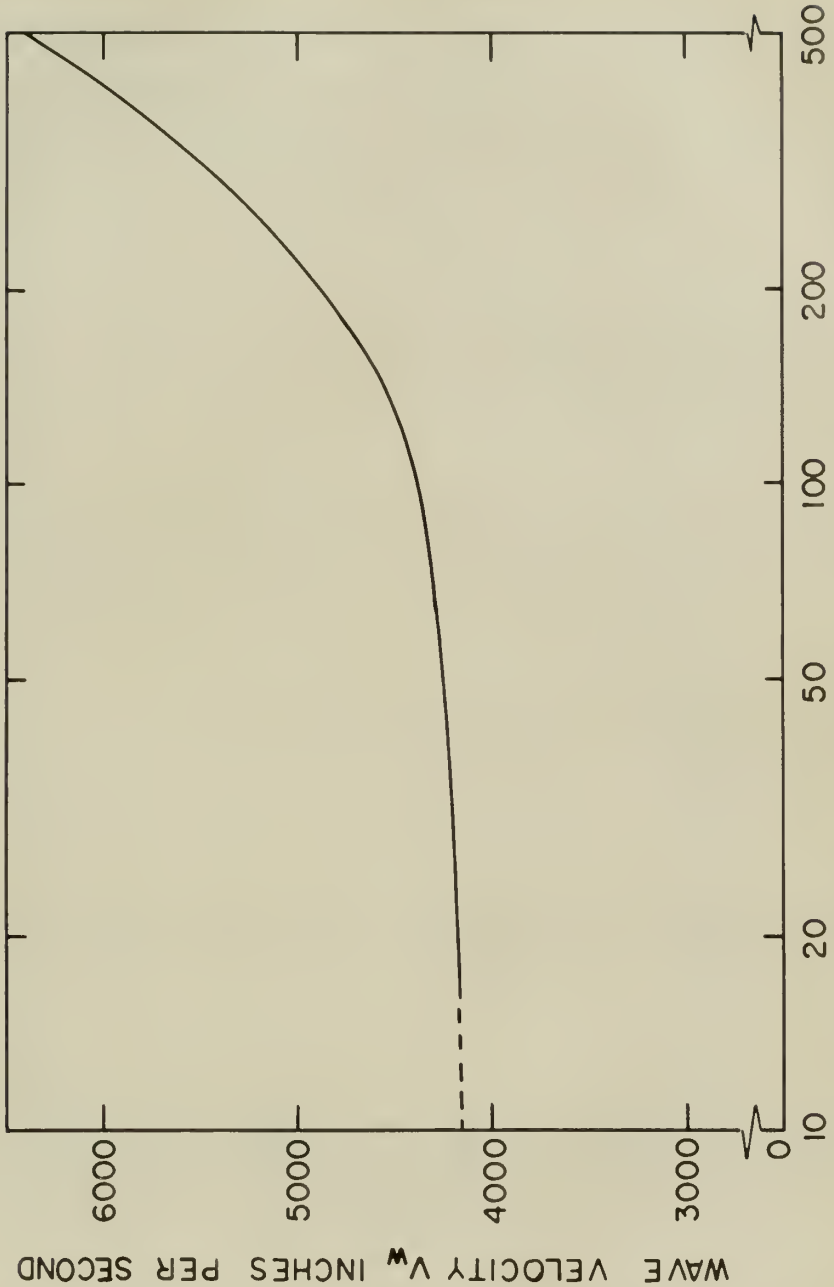

Figure 6. Wave velocity versus frequency

Figure 7. Variation of the parameter ρ_R with oscillator frequency

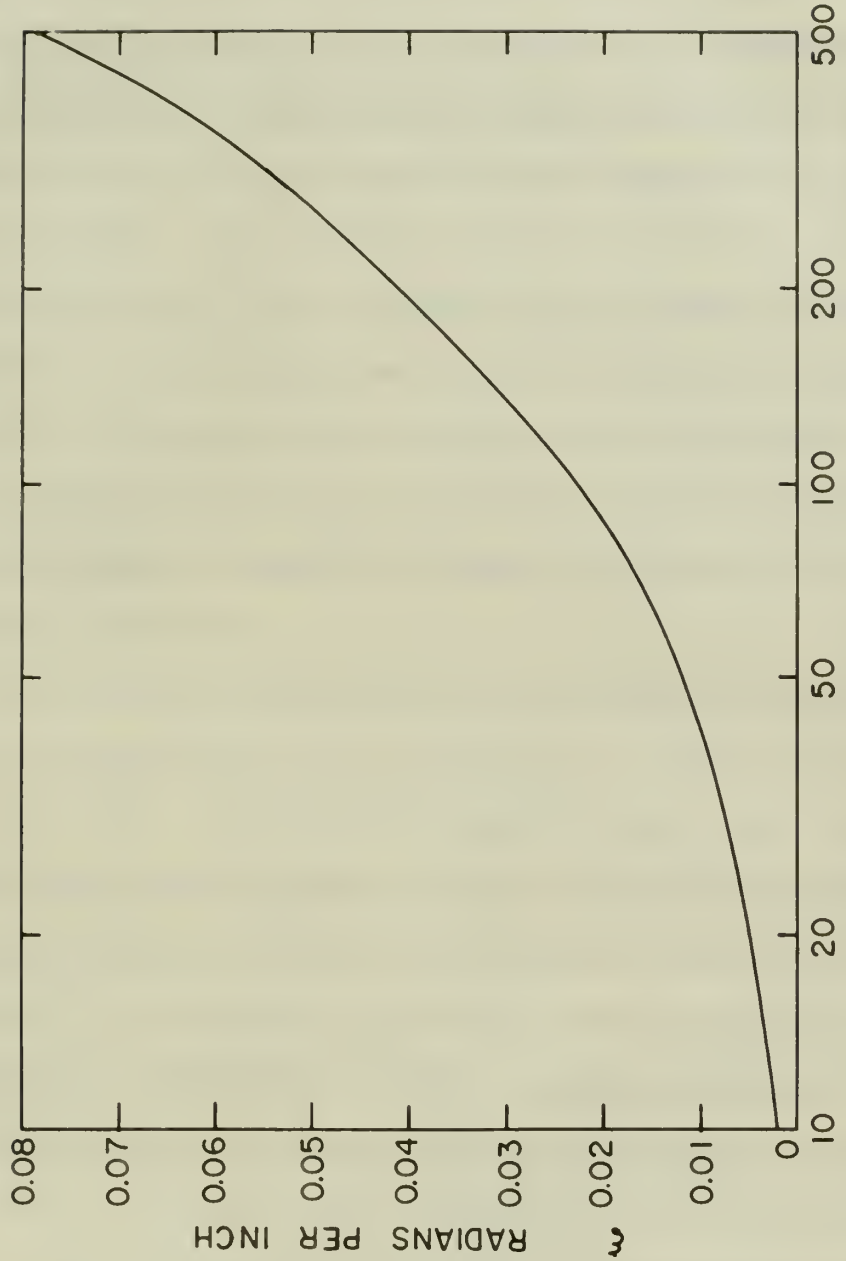

Figure 8. Variation of the parameter ε with oscillator frequency

length of the steady component, γ, is a constant equivalent to ρ_R at zero frequency. One of the parameters of importance relates the difference between the values ρ_R and γ. This difference is greater for high oscillation frequencies.

The initial attempt consisted of an analysis of the counts of four scalars, each of which counted for oscillator periods of 180°. Each counter however counted a separate period, differing by 90° or 180° from the other counters. In order to obtain a high oscillator frequency, a double sine pattern was glued onto the rotating oscillator drum and the disc was machined for the appropriate sequence, in this case, cutting the light every 90° of drum rotation, or 180° of oscillator rotation.

Due to system irregularities, the plan to use four scalars in conjunction was abandoned, and only two scalars were used. This required two runs for each set of data taken. Although the signal output from the coincidence-anti-coincidence circuit was of a distinct and consistent square shape, some of the scalar discriminators were quite sensitive to extraneous influences and had a rather profound effect on the counting rate. Further, the discriminators seemed to exhibit drift which further compounded the difficulty. Eventually, it was necessary to use only two scalars as the slave scalars. One of these scalars, the Nuclear-Chicago Ultrascalar, had no discriminator, while the discriminator

on the other scalar, a Baird-Atomic unit was quite insensitive except at each extreme. Both proved to give reproducible results.

It was also necessary to replace the double sine pattern with a single pattern while the associated timer was changed to cut the light beam at each 180° of both drum and oscillator rotation.

A direct analytical approach was devised to determine the phase lag and sinusoidal amplitude. The variation of the flux within the subcritical assembly was considered to be composed of a steady state component with a sinusoidal component superimposed upon it. The flux at any point will be proportional to the counting rate at that point. At the source, the counting rate can be expressed as

$$R = R_s + R_w \sin \frac{2\pi}{T'} t \qquad (43)$$

where R is the total counting rate, R_s is the steady state counting rate, R_w is the relative amplitude of the sine wave expressed as a counting rate, and T' is the period associated with the sinusoidal wave. At any point other than the source, the count rate can be expressed as

$$R = R_s + R_w \sin \left(\frac{2\pi t}{T'} - \theta \right) \qquad (44)$$

where the R values are peculiar to the point being investigated, and the lag angle is θ.

It is desired to find the value of R_w and θ by experimental methods.

Figure 9 shows the count rate as indicated at the source (Figure 9a), and then as it would be at some point in the assembly with a lag angle θ (Figure 9b and c).

In the original design, four scalars were electronically switched so as to count only during the periods indicated by the cross hatched areas lettered A, B, C, and D. The areas A and C are associated with one photocell, while the areas B and D are associated with the other cell. The areas themselves represent the total counts recorded during the period associated with each area, or 180° of cycle duration.

To obtain the total counts per cycle in area A, integrate the counting rate Equation 44 between the appropriate limits, 0 and $\frac{1}{2}T'$

$$A = \int_0^{\frac{1}{2}T'} R_s \, dt + \int_0^{\frac{1}{2}T'} R_w \sin\left(\frac{2\pi t}{T'} - \theta\right) dt \qquad (45)$$

$$A = \tfrac{1}{2} R_s T' + \frac{R_w T'}{\pi} \cos\theta \qquad (46)$$

For n cycles, the total number of counts registered during the A interval is

$$N_A = \tfrac{1}{2} R_s T'n + \frac{R_w T'n}{\pi} \cos\theta \qquad (47)$$

Similarly, for the other intervals

$$N_B = \tfrac{1}{2} R_s T'n + \frac{R_w T'n}{\pi} \sin\theta \qquad (48)$$

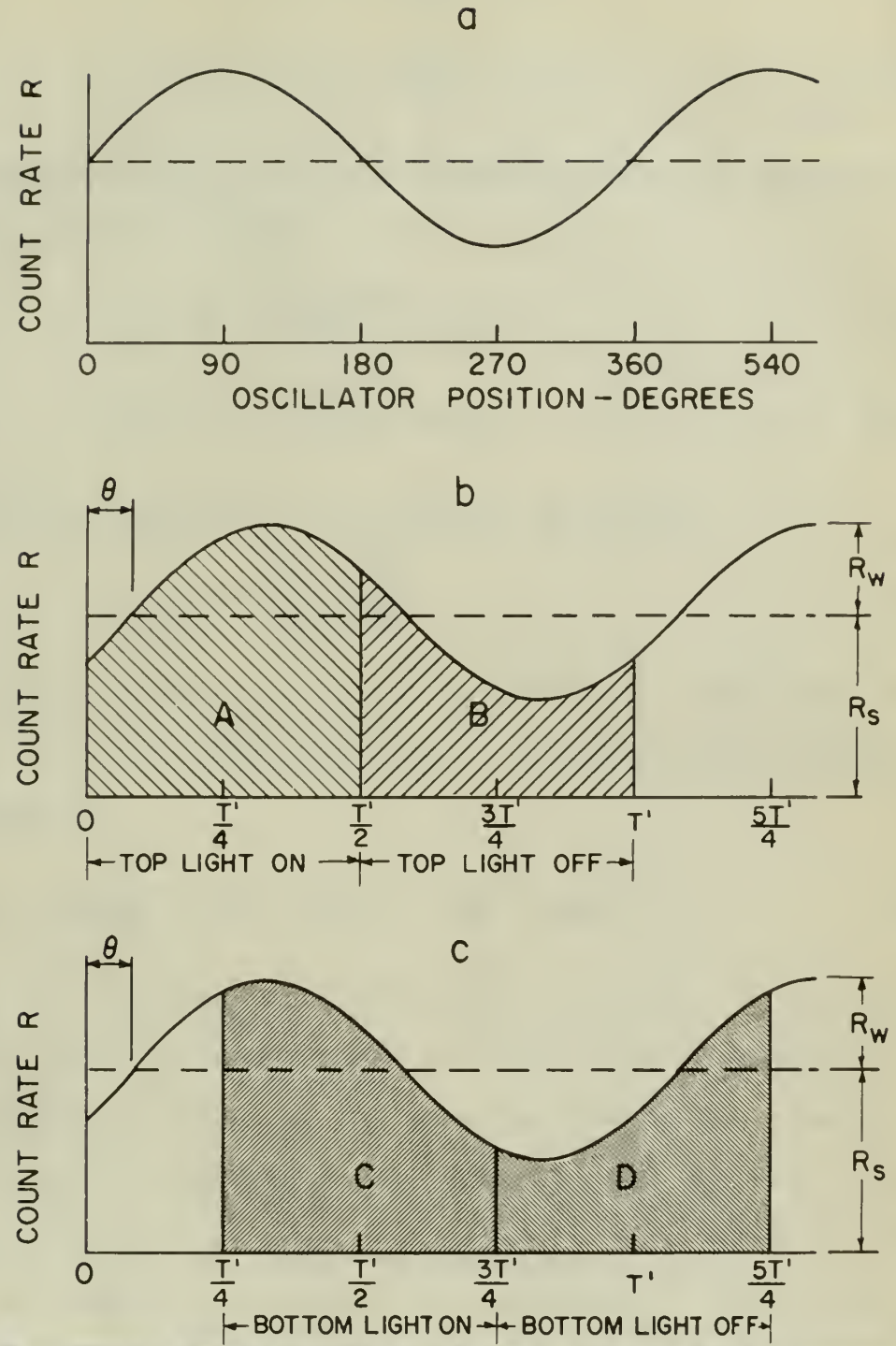

Figure 9. Phase and counting relationships at the source and at some point in the assembly

$$N_C = \tfrac{1}{2} R_s T'n - \frac{R_w T'n}{\pi} \cos \theta \qquad (49)$$

$$N_D = \tfrac{1}{2} R_s T'n - \frac{R_w T'n}{\pi} \sin \theta \qquad (50)$$

Subtraction of Equation 50 from Equation 48 and Equation 49 from Equation 47 yields

$$N_B - N_D = \frac{2 R_w T'n}{\pi} \sin \theta \qquad (51)$$

$$N_A - N_C = \frac{2 R_w T'n}{\pi} \cos \theta \qquad (52)$$

Division of Equation 51 by Equation 52 yields

$$\text{Tan } \theta = \frac{N_B - N_D}{N_A - N_C} \qquad (53)$$

from which the phase angle may be obtained. Equations 51 and 52 can be solved simultaneously to determine the relative amplitude, or

$$R_w = \frac{\pi}{2 nT} \left[(N_B - N_D)^2 + (N_A - N_C)^2 \right]^{\frac{1}{2}} \qquad (54)$$

It is seen that by knowing the count rate of the four scalars, both the phase angle and the relative amplitude of the wave may be found at any position within the assembly.

In order to determine the precision of the data taken, evaluation of the standard deviation in each value of phase angle and relative amplitude was calculated. The method used to derive these standard deviations is given in Appendix D.

$$\frac{\partial^2}{\partial x^2} + \frac{\partial^2}{\partial y^2} + \frac{\partial^2}{\partial z^2} = \frac{1}{c^2}\frac{\partial^2}{\partial t^2} \qquad (24)$$

$$\frac{\partial^2}{\partial x^2} + \frac{\partial^2}{\partial y^2} + \frac{\partial^2}{\partial z^2} = \frac{1}{c^2}\frac{\partial^2}{\partial t^2} \qquad (25)$$

Substitution of Equation 23 into Equation 24 and Equation 25 then Equation 24 yields

$$\frac{\partial^2}{\partial x^2} + \frac{\partial^2}{\partial y^2} + \frac{\partial^2}{\partial z^2} = \frac{1}{c^2}\frac{\partial^2}{\partial t^2} \qquad (26)$$

Division of Equation 26 by Equation 25 yields

$$\frac{\partial^2}{\partial x^2} + \frac{\partial^2}{\partial y^2} + \frac{\partial^2}{\partial z^2} = \frac{1}{c^2}\frac{\partial^2}{\partial t^2} \qquad (27)$$

$$\tan\theta = \frac{\partial^2 - \partial^2}{\partial^2 - \partial^2} \qquad (28)$$

Then either the above ratio may be considered. Equations 2 and 3 can be solved simultaneously to determine the relative amplitudes:

$$\partial^2 + \frac{1}{2}\partial^2 \left[(\partial^2 - \partial^2)^2 + (\partial^2 - \partial^2)^2\right] \qquad (29)$$

It is then easy to evaluate the energy density of the field existing, from the above ratio. The relative amplitudes of the wave may be found if any particular energy is assumed.

In order to evaluate the reflection of the wave, consideration of the dynamic interaction of such waves of light with matter may prove helpful. The method used by Bohr (Bohr, 1913) utilizes the quantum theory. The method used by Bohr is to consider the energy of

B. Typical Run

As counts are taken at points further from the source, the count rate decreases due to attenuation. In order to keep the statistical deviation approximately constant throughout, the length of counts was varied from a minimum of 4 minutes in the lower row of channels to a maximum of 80 minutes in the upper (59") row. Further, in most channels, a series of runs was completed in an effort to avoid random variation.

A typical run was conducted as follows. About an hour or more prior to the run, the equipment was turned on and allowed to warm up. Each slave counter was run for a two minute interval and its count compared with the count of the master scalar. Highest variation encountered was 12 counts on a total count of 60,000. The chain was then disconnected from the oscillator, the motor was engaged so as to turn the light chopper, and a two minute count was taken with the electric timer channeling the counts to the two scalars, but with the oscillator stationary. As this caused a steady source of neutrons to stream up the assembly, both of the slave scalars should read approximately equivalent quantities, and the total of the slave scalars should approximate the reading of the master scalar. These readings, in the final arrangement of Baird-Atomic and Nuclear Chicago scalars, were invariably within statistical standard deviation limits.

The chain was then reassembled and the location of the timer cutting edge verified in relation to the cadmium pattern on the oscillator. The motor was then restarted and the oscillator allowed to reach a steady speed.

The count was started for the first run. During the first run, the speed of revolution of the oscillator was checked with a revolution counter. This was checked again near the end of that series of runs. Speed control was within 2 rpm of a total of 506 rpm.

At the completion of the first count in any given hole, the drive chain was broken and reset on the sprocket 90° away from its previous setting. The motor was again engaged and the count for that channel completed.

In order to make a comprehensive survey of the wave in the assembly, counts were conducted in two of the columns and in three of the horizontal rows. The main portion of the data was taken at a speed of 506 rpm. One run however was conducted at 1,308 rpm. At this speed, vibration of the oscillator was considered excessive and it was not considered prudent to prolong experimentation at this speed. Single readings were taken for channels 1c, 2c, 3c, and 4c and these data were evaluated.

VII. RESULTS

The theory predicts primarily two things: a neutron wave in a subcritical assembly travels at a finite velocity in the assembly, thus exhibiting a phase lag at points away from the source; and the attenuation of the wave amplitude differs from the attenuation of the steady state, hence this variation can be used to determine other qualities of the assembly.

The data taken from all recording runs are given in Appendix A. By substitution in Equations 53, 54, and D10 and D15 in Appendix D, the values of the phase lag, relative wave amplitude, and the statistical standard deviation in these two quantities were determined. These data have been presented in Appendix B.

One of the parameters of prime importance was the variation of wave amplitude with distance up the assembly. When plotting the relative counting rate versus distance on semi-logarithmic paper, a straight line should result. The slope of this line is directly related to the inverse attenuation length of the wave, γ_R in the theory propounded. This inverse relaxation length is different from the inverse relaxation length of the steady component γ, and in this difference lies one object of investigation.

The relative wave amplitude of the wave at 506 rpm was plotted for columns b and c as shown in Figures 10 and 11 respectively. In each case, straight lines were drawn con-

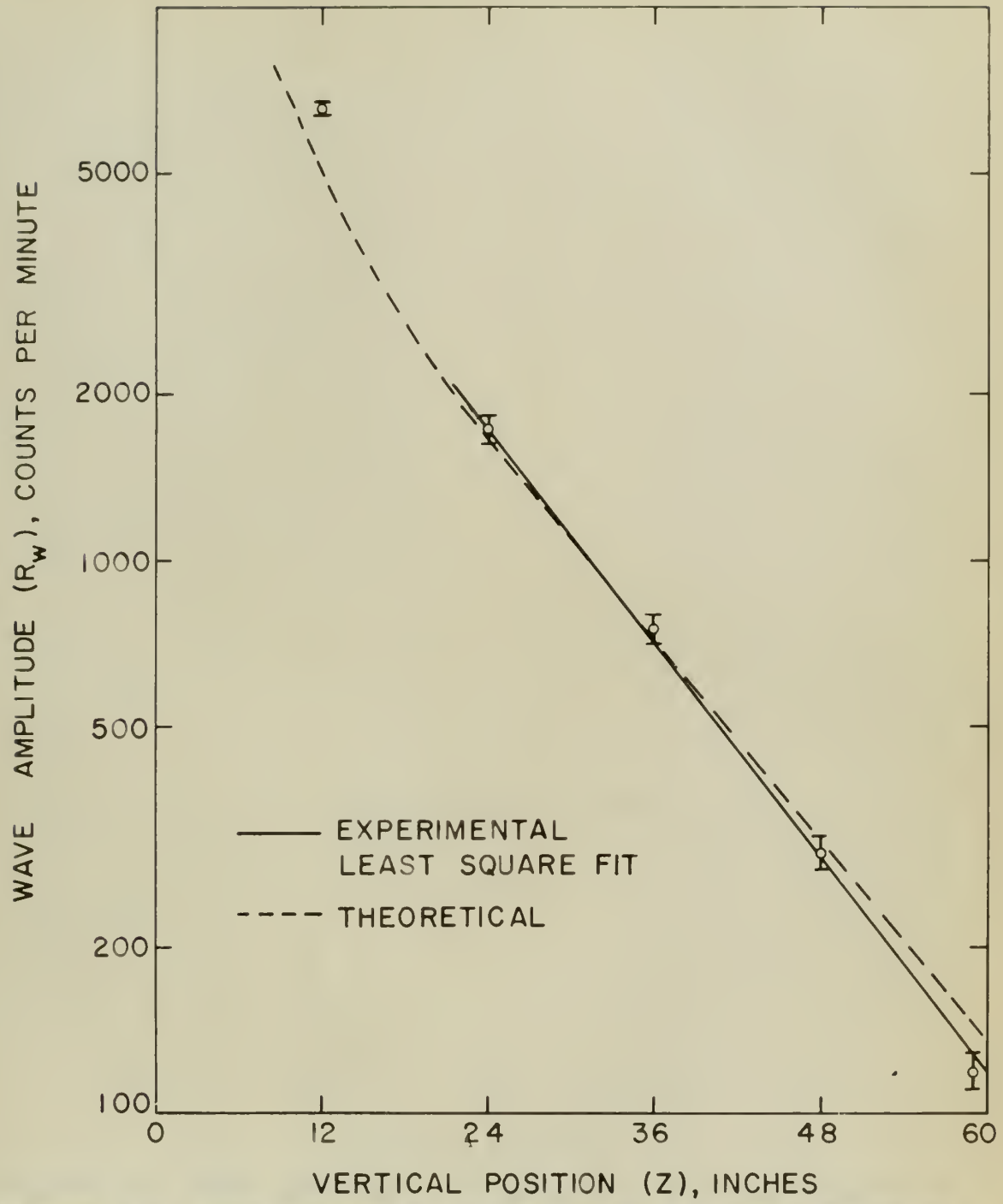

Figure 10. Wave amplitude in column b, 12 inches south of centerline, 506 rpm

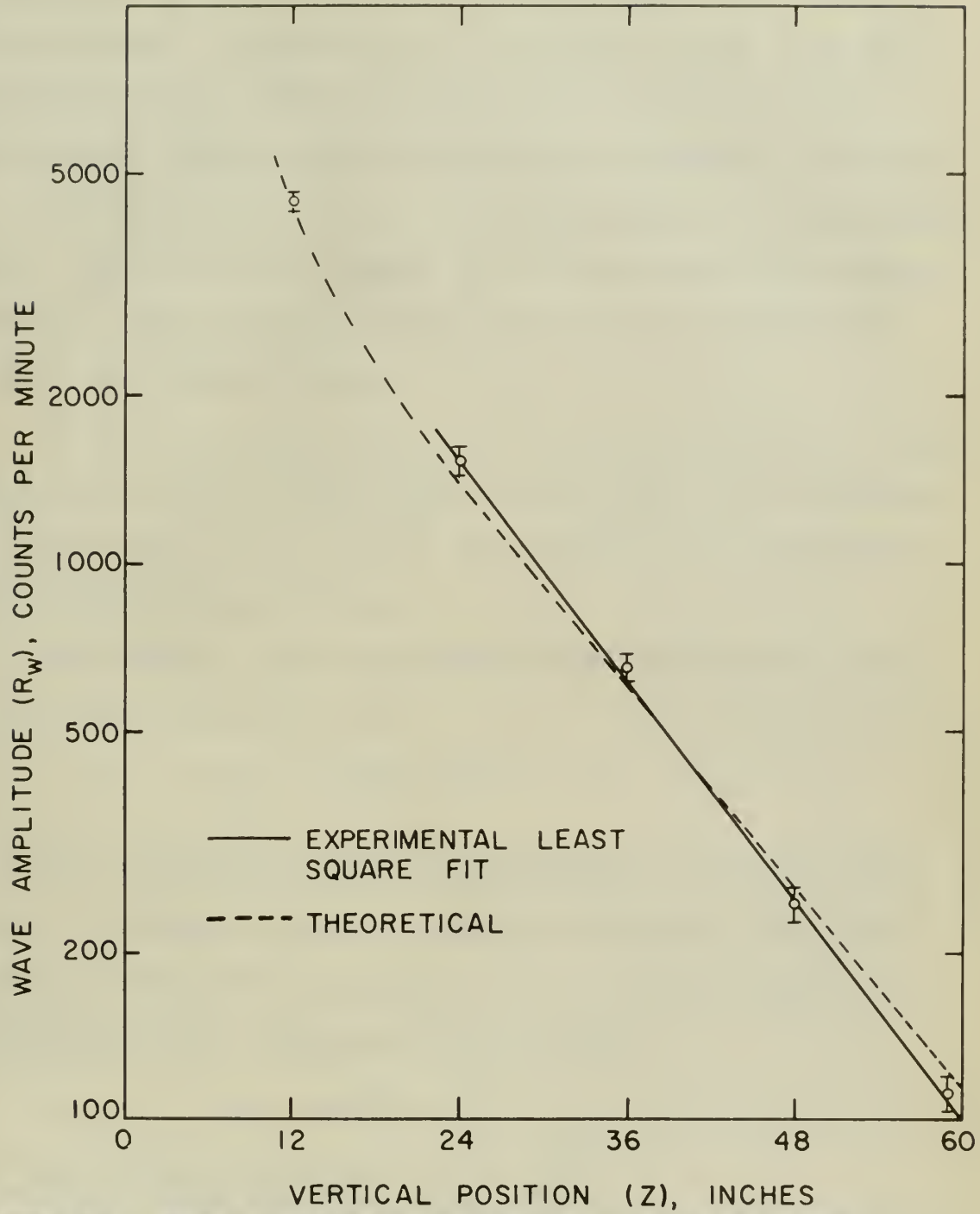

Figure 11. Wave amplitude in column c, on centerline, 506 rpm

necting the points associated with the upper four channels of the column. In Appendix C, the effect of the flux contributions of the higher harmonic modes is investigated. Theoretical considerations forecast an increase in amplitude in the bottom channel due to the contribution of these higher modes. This forecast appears to have been verified, and as a result, the experimental line has not been extended to include the bottom channel.

It is to be noted that in all figures, the dotted lines, which are plots of theoretical calculations, are indicative of slope only, and are not to be construed as representing quantitative measurements.

For column c, the experimental wave inverse relaxation length was determined to be

$$\rho_R = 0.0762 \text{ in}^{-1}$$

While the correlation between theoretical and experimental curves in Figures 10 and 11 compares favorably within the limits of statistical deviation, the two values found vary considerably, the theory yielding a value

$$\rho_R = 0.0689 \text{ in}^{-1}$$

an error of approximately 9.5 per cent.

For column b, the experimental value of the inverse relaxation length was

$$\rho_R = 0.0751 \text{ in}^{-1}$$

quite close to the experimental value found for column c. The theory indicates that these values of ρ_R for columns b and c should be identical. The magnitude of deviation from theoretical considerations is somewhat excessive.

The amplitude of the wave at high speed (1308 rpm) is shown in Figure 12 as a function of the vertical distance z, readings being taken in column c, on the centerline. The inverse relaxation lengths were determined to be

$$\rho_R = 0.0663 \text{ in}^{-1} \quad \text{- Experimental}$$
$$\rho_R = 0.0742 \text{ in}^{-1} \quad \text{- Theoretical}$$

about 10.5 per cent deviation, but with the theoretical value lower than the experimental, the reverse of the findings at low speed. The high speed runs may be looked upon skeptically, as they were only conducted one time. However, the indication is worthy of note.

The other parameter of prime interest is the value of ξ, or the slope connected with the plot of phase lag versus vertical position. The phase lag at various positions in column b is shown in Figure 13, while the lag at positions in column c is shown in Figure 14. Both of these surveys were conducted at 506 rpm.

Theory forecast that the phase shift should be identical for these cases. The slope of the curves is the quantity ξ. In both cases, the experimental slope of lag versus assembly

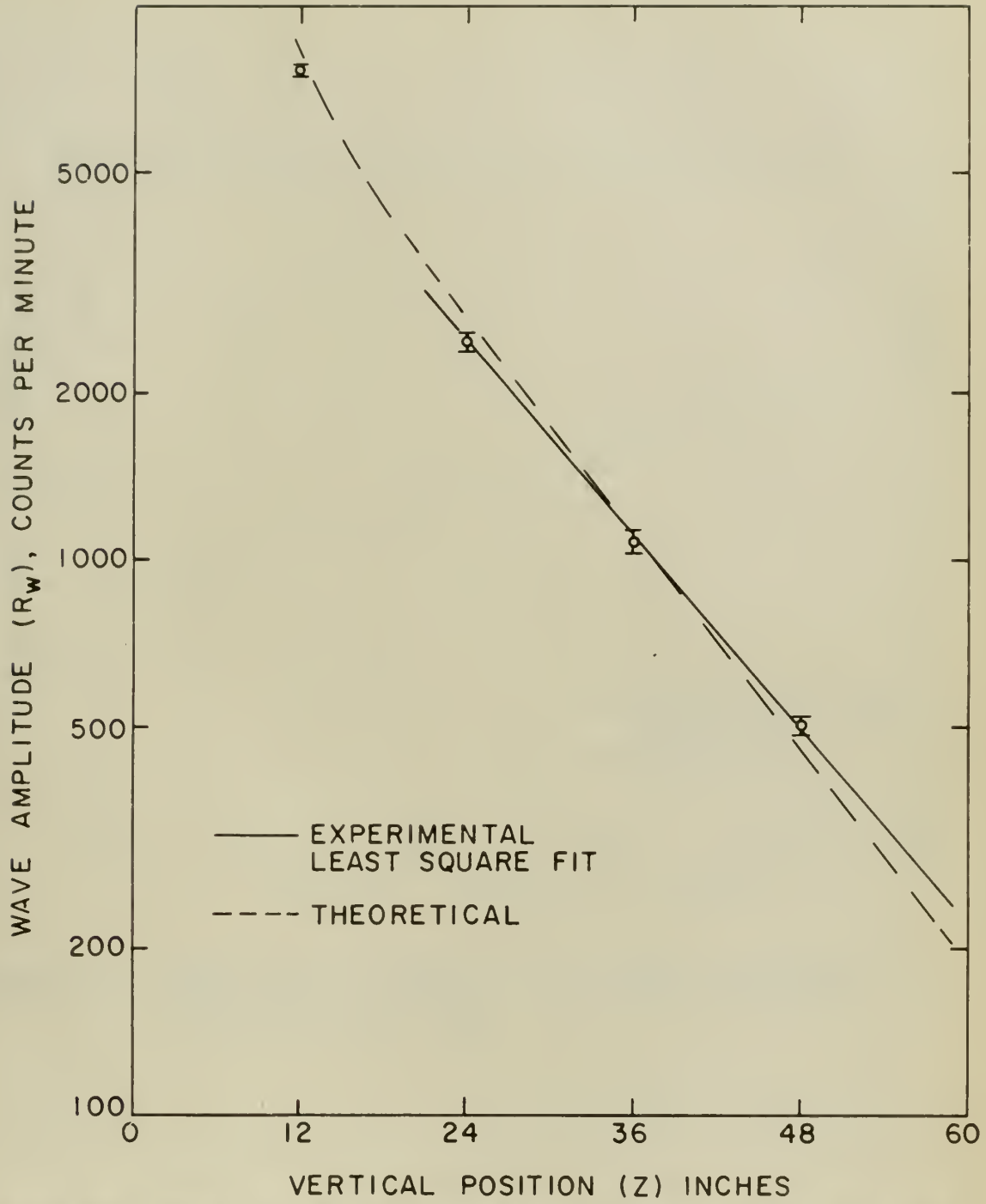

Figure 12. Wave amplitude in column c, on centerline, 1308 rpm

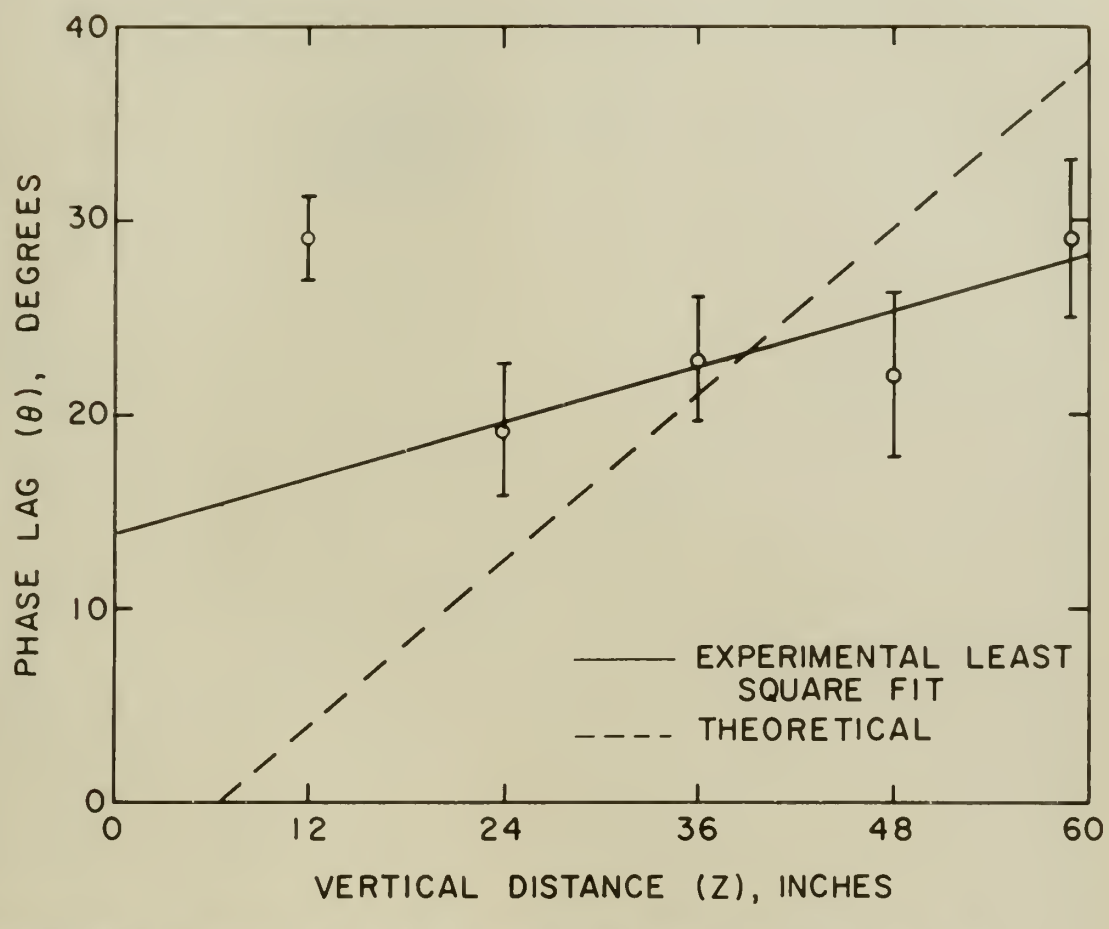

Figure 13. Phase lag in column b, 12 inches south of centerline, 506 rpm

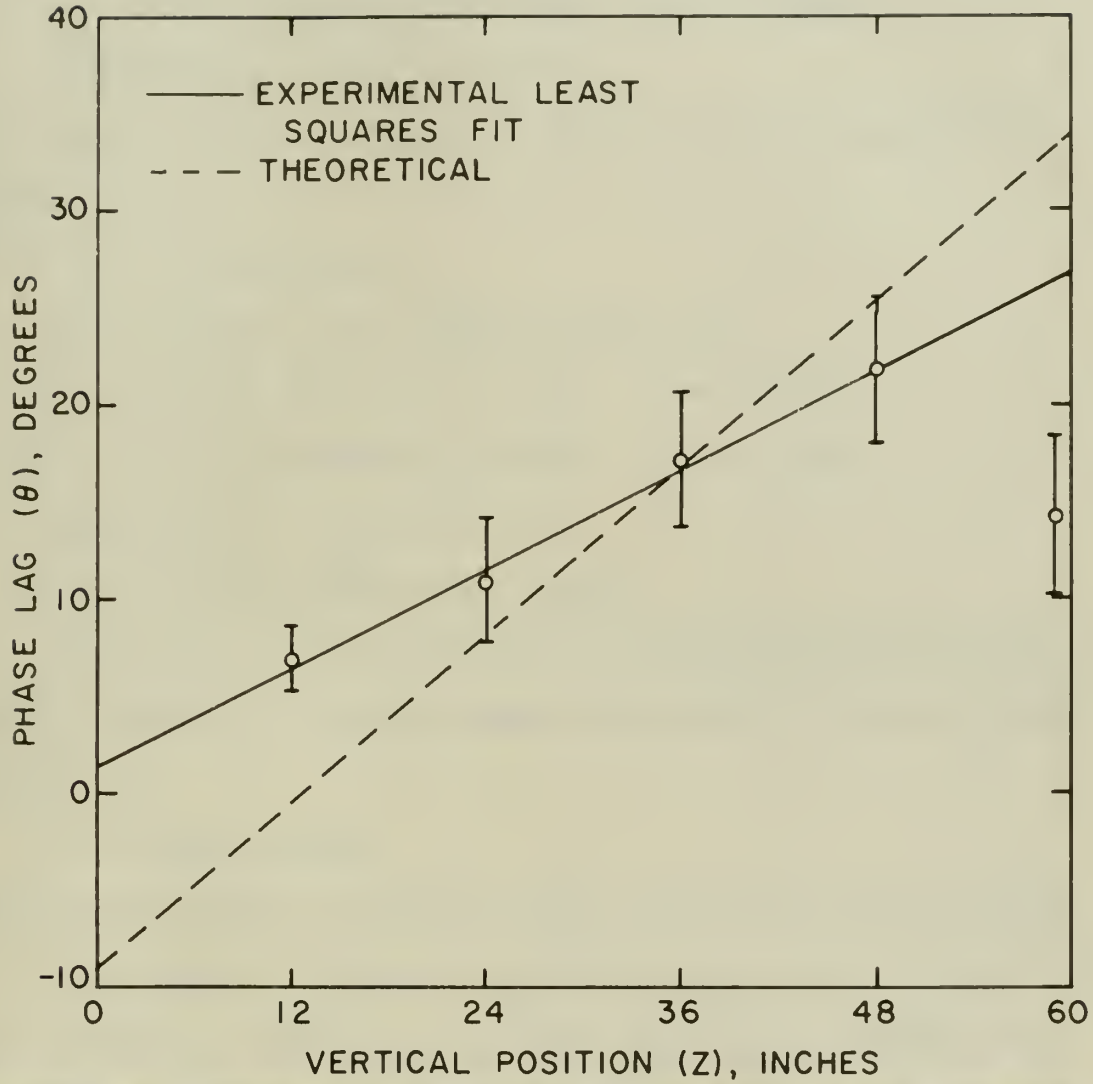

Figure 14. Phase lag in column c, on centerline, 506 rpm

height was less than forecast. The values of ξ for column c were

ξ = 0.710 degrees per inch - Theoretical.

ξ = 0.425 degrees per inch - Experimental.

Difference = 40.3 per cent.

The experimentally determined value of wave velocity for column c was

V_w = 7,142 in/sec.

For column b, the values found were

ξ = 0.710 degrees per inch - Theoretical

ξ = 0.240 degrees per inch - Experimental

Difference = 66.2 per cent

V_w = 12,648 inches per second.

The value of the diffusion coefficient was calculated using Equation 41 and the data for column c, and was found to be

D = 0.534 inches

This value should be viewed with considerable skepticism.

The value of material buckling found using Equation 42 was negative. This is in disagreement with previous measurements and has not been included.

Figure 15 is a plot of the phase lag versus height for the high speed run, and this deviates even farther from the forecast phase lag.

In an attempt to explain the deviations of experiment

Weight one Inch Cube Specimen:- The values of $\frac{1}{2}$ for solids
& gases

$\frac{1}{2}$ = 0.312 Degrees per Inch - Theoretical.

$\frac{1}{2}$ = 0.340 Degrees per Inch - Experimental

Difference = 8% for Gases.

The quantitative Investigation which we have undertaken for
Gases & Gas

K^0 = 1.710 Calories.

The values θ^0 for various Gases were

$\frac{1}{2}$ = 0.312 Degrees per Inch - Theoretical

$\frac{1}{2}$ = 0.340 Degrees per Inch - Experimental

Difference = 8% for Gases

K^0 = 1.710 Calories per second.

The value of the Diffusion coefficient was calculated
under equation 7) and the data for values θ, and the final
be be

= 0.425 Grams

Data value agreed to within 10% considering Simplifying.

The value of Specific Gravity Gases using Equation 7)
are accurate. This is in Contradiction with Lorentz empir-
ically and Gas Law Gases Calories.

Chapter II is a Plan of the Gases Its Purpose Method Gas
Gas High Speed and Its Gas Gases Investigation Gases Diffusion
Gases Gases Two.

In an Example We apply the Simplifying Of Equations

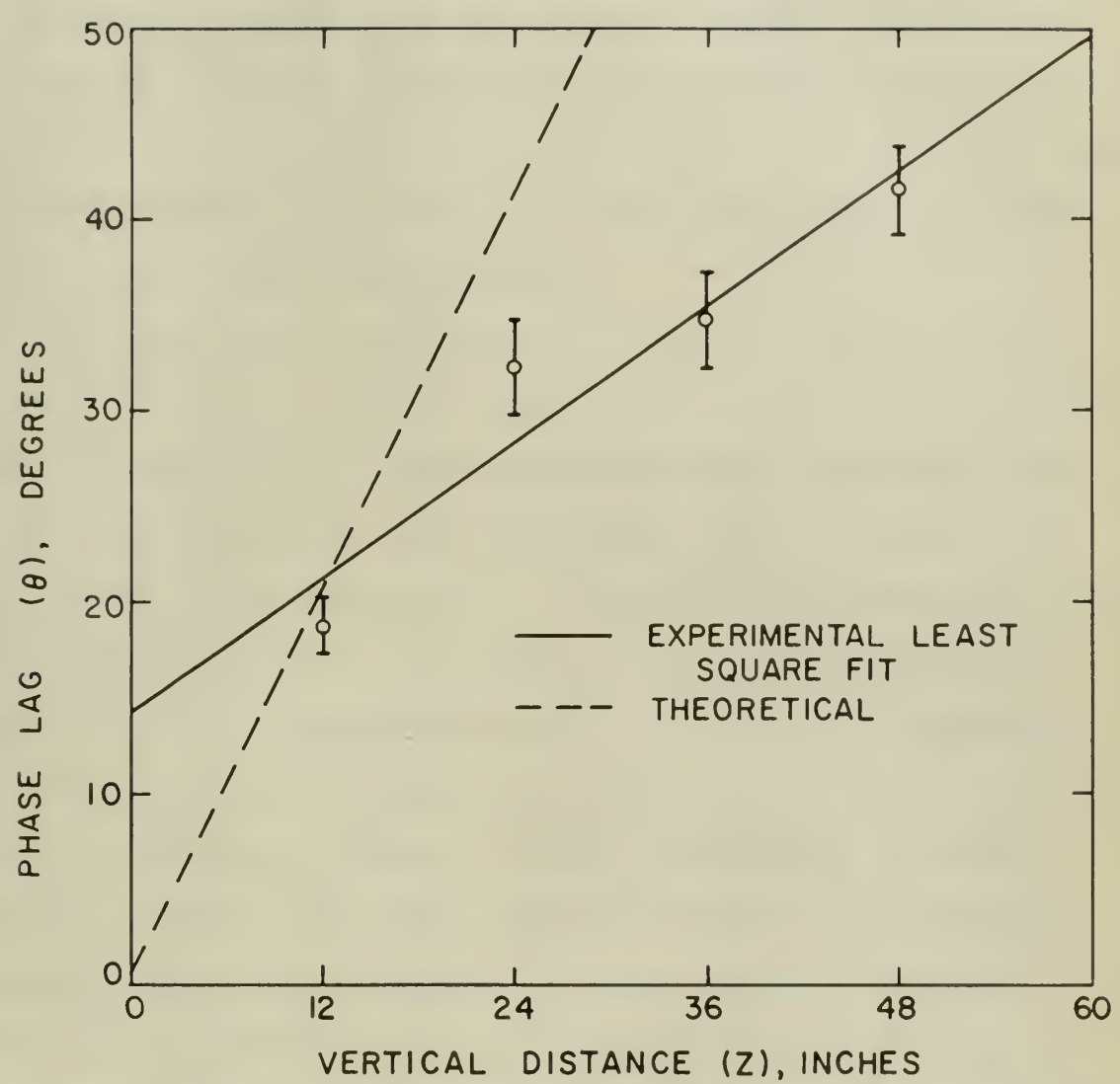

Figure 15. Phase lag in column c, on centerline, 1,308 rpm

from theory, additional phase and amplitude studies were conducted at various points in the assembly.

In Figure 16 is plotted the wave amplitude as a function of horizontal position at three height levels. The curves are cosine curves with amplitude corresponding to the maximum amplitude at the center. It is to be seen that the amplitude agrees with the theoretical prediction of a cosine distribution of flux within the assembly.

In Figure 17, the phase lag at various levels in the assembly is shown. In all cases, theory predicts that these should be horizontal lines indicating equal lag within each level. It is obvious that this state does not exist until the fourth row is approached. A non-rigorous explanation of this phenomenon can be theorized. The oscillator allowed neutron egress through the top 180° of its arc of rotation. In the theoretical derivation, a point source was stipulated. As the oscillator rotates, it has a directional tendency, allowing neutrons to exit in line with the open area of the pattern. The pattern rotates in such a manner that exit areas are opened in a sidewise direction before reaching a vertical direction. Thus some neutrons, exiting just after the minimum has been passed, will reach the northernmost area of the assembly, i.e., column e, before the reference time, as noted on the centerline, i.e., column c. This would explain how channel 2e of Figure 17, exhibits a phase lead;

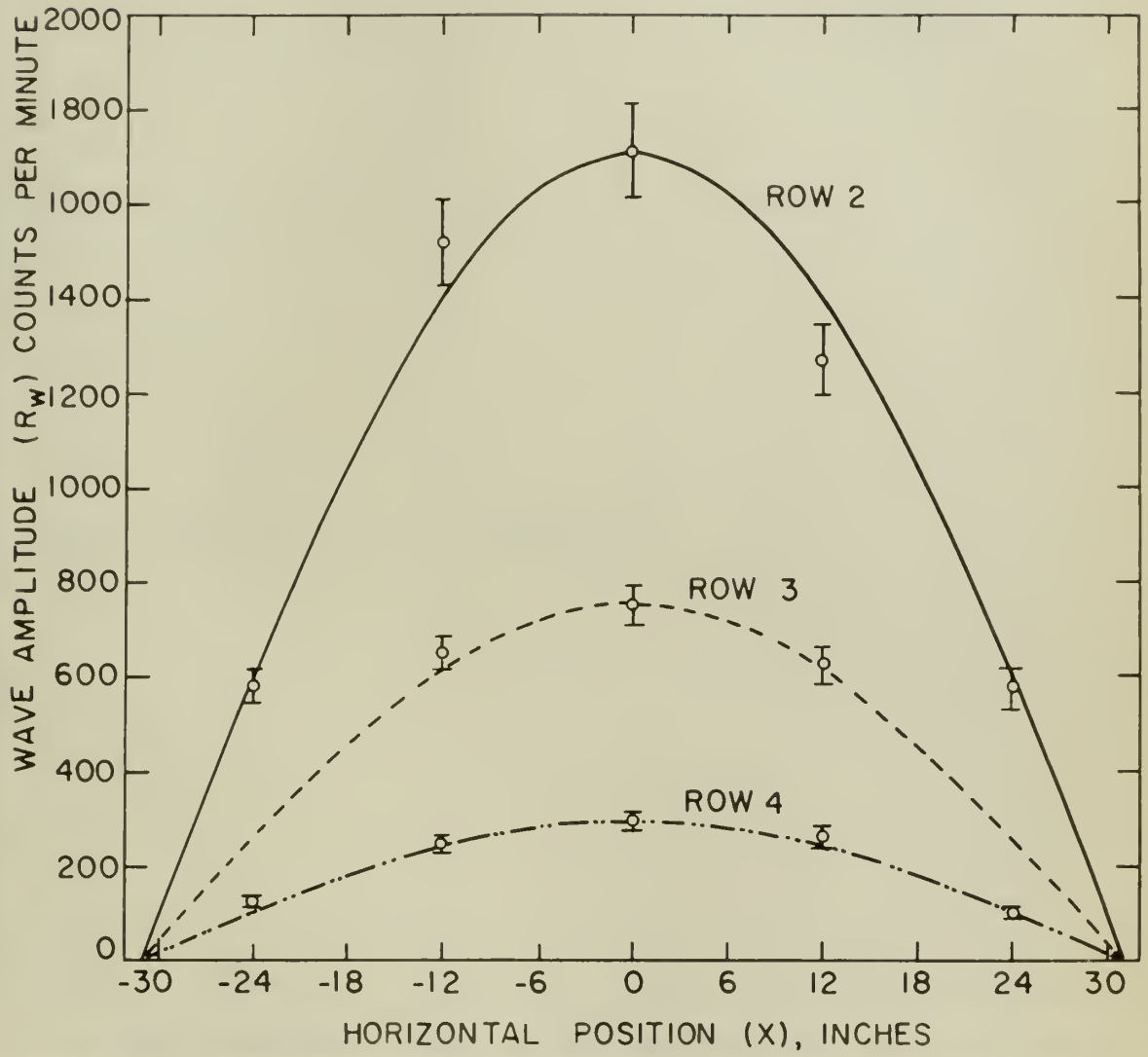

Figure 16. Wave amplitude at the 24, 36, and 48 inch levels

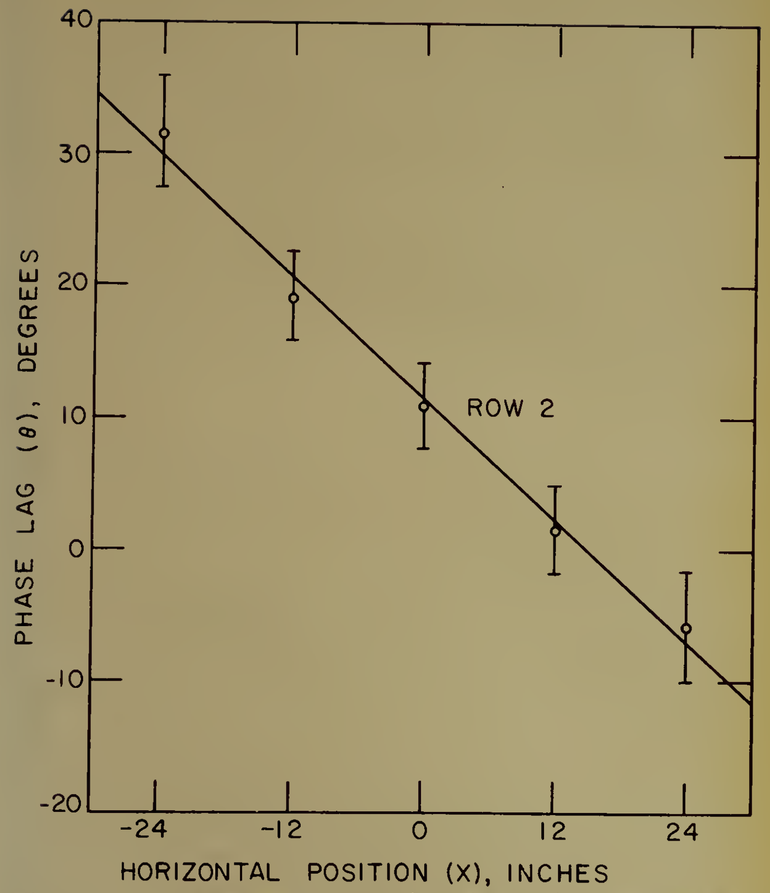

Figure 17. Phase lag at the 24, 36, and 48 inch levels

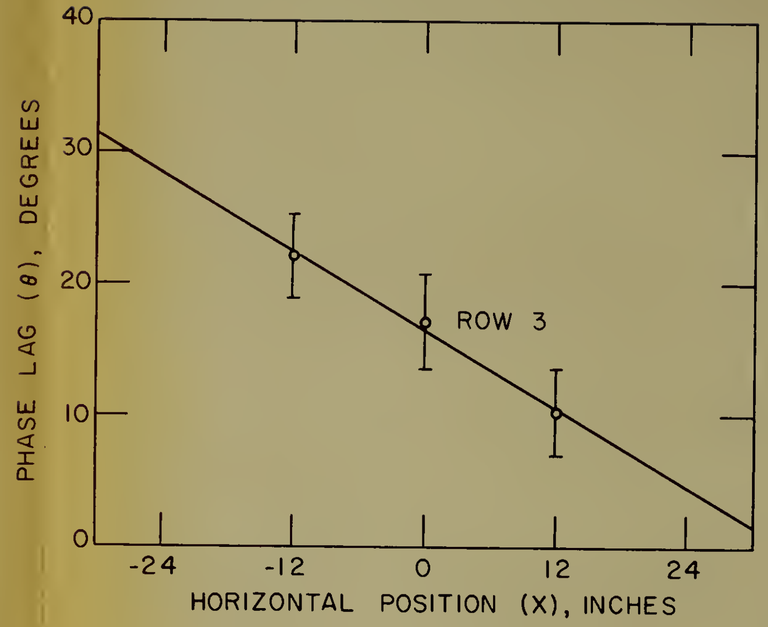

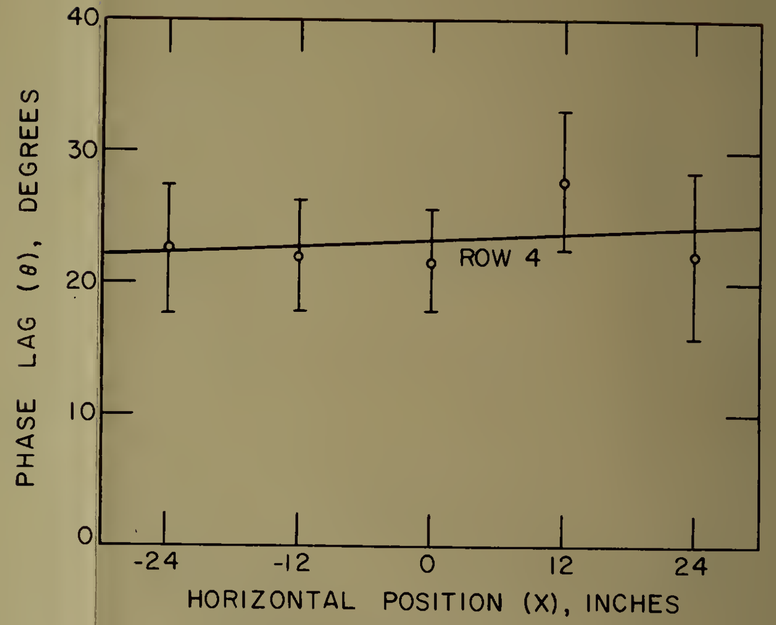

and, consequently the remaining portion of the curves for rows 2 and 3. As the neutrons progress up the assembly, the diffusion tendency is to exit toward the areas of low neutron density, thus leveling off the curve at higher levels. This phenomenon associated with the oscillator, will aid considerably in explaining the difference in slope of the θ versus z curves for column b and c (see Figures 13 and 14). If the directional quality of the neutron beam were not present, the lag of the lower three channels of column b would be considerably less, causing the slope of the experimental line to approach the theoretical curve more closely. This also illustrates the fact that any readings taken to determine ρ_R or ξ must be taken on the centerline of the assembly.

In order to verify that the flux did indeed vary sinusoidally throughout the assembly, one minute counts were taken in channels 1c, 3c, and 2a, while rotating the oscillator drum in ten degree increments. This "static" calibration is shown in Figure 18, and it is to be seen that the flux distribution does indeed follow a sinusoidal pattern.

The effect of the end correction factor was investigated. For the area investigated, the end correction factor was found to take on a value of 0.941 for the fifth row. All other channels exhibited end correction factors greater than 0.99.

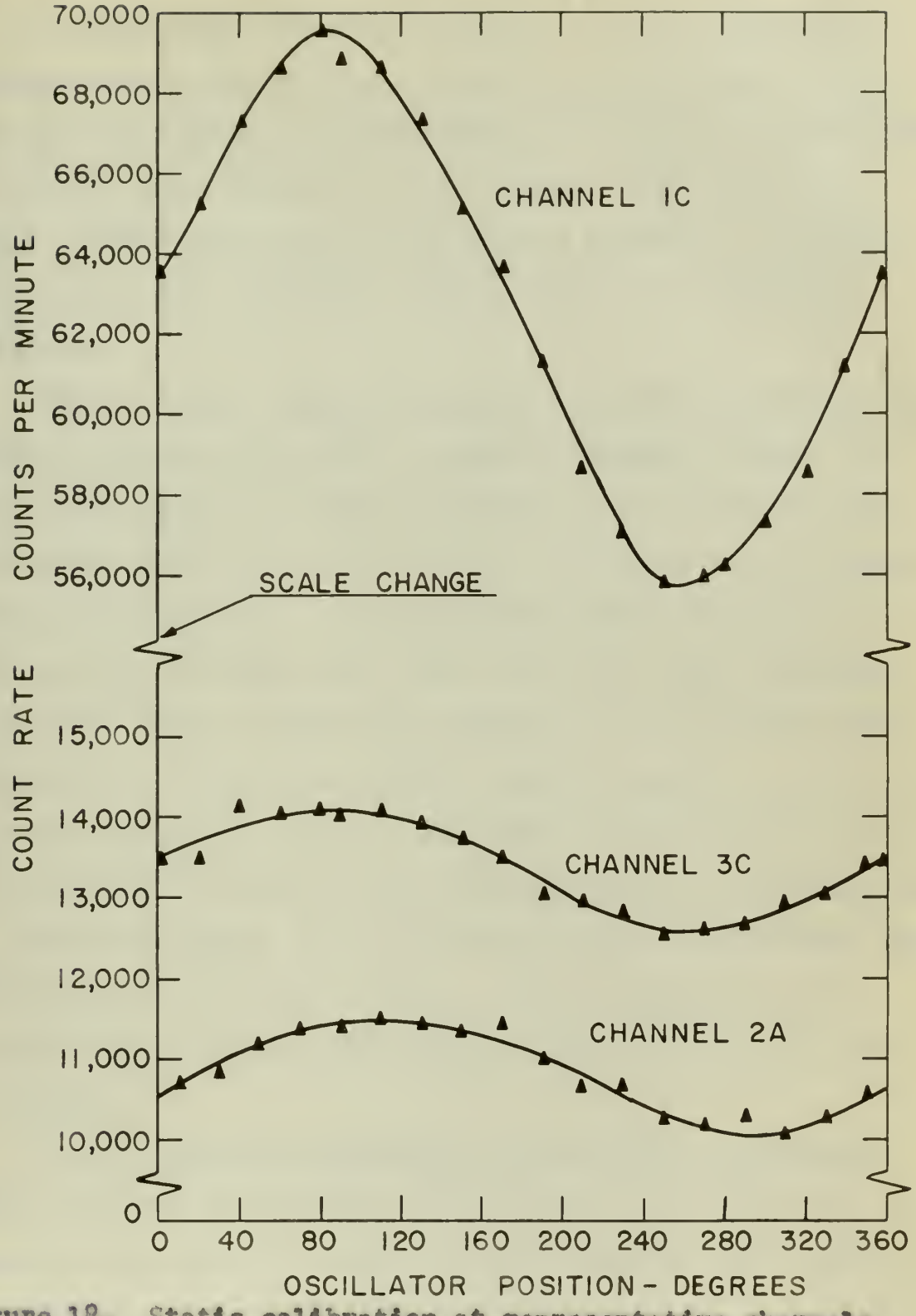

Figure 18. Static calibration at representative channels

In evaluating the overall results of the experiment, several things are evident. In all cases, the value of ξ_0 was less than forecast, which indicates that the wave velocity is greater than predicted by the theory. While the data taken at high speed are not considered reliable, it did indicate that this deviation between theory and experiment broadens.

There is some reason to believe that the experiment was carried out over too broad a range of assembly height. In the lower regions, the flux consists of some neutrons from the source which were not included in the original diffusion equation, Equation 3. A tendency has also been noted for the curve of θ versus z to level off at the upper extremes, indicating that the wave like qualities of the neutron wave disappear at a moderate distance from the source. It is of interest along this line of reasoning to note that Kaievski and Horowitz (4) limited their investigations to approximately 30 inches of medium, and experienced slight fluctuations from statistics at the outer extreme. These experiments were carried out at considerably higher speed, between 4800 and 15,000 rpm.

While the wave attenuation agreed within experimental error with the theoretical considerations, the deviation was too great to arrive at values for the buckling and diffusion coefficient. The correlation of the theory and experimental

attenuation lengths was less distinct at the high frequency investigated, although again, the data taken at this speed are subject to considerable doubt.

VIII. CONCLUSIONS

A theoretical and experimental study was undertaken to determine the characteristics of neutron waves within the natural uranium - graphite subcritical assembly of the Iowa State University, and from this information, determine the diffusion coefficient and the buckling of the assembly.

As a result of this study, it was found that:

(1) Neutron waves do exist in the assembly when an oscillating source is introduced. Furthermore, these waves do follow the tendency forecast by the theory.

(2) The wave velocity in all cases investigated was higher than forecast by the theory. There was some indication that the deviation became greater as the oscillator frequency was increased.

(3) At high frequencies, the correlation between theory and experiment becomes even less distinct. It is speculated that the position investigated should be limited to the range of heights between 15" and 40".

(4) Though the phase and amplitude measurements agreed moderately well within experimental error, the correlation was not sufficiently close to determine a value of the buckling or diffusion coefficient of the assembly.

VIII. CONCLUSION

A theoretical and experimental study was undertaken to determine the characteristics of reactions among ultimate the natural bacteria - coagulin equilibrium assembly of the Iowa River Delaware, and rose city information; determine the different quantities and the Duration of the assembly.

In a result of this study, it was found that:

(1) Reaction curve do exist in the assembly when an unfailing reaction is determined. Therefore, there were to follow the laboratory discussed by the theory.

(2) The Iowa Velocity in all cases investigated may differ when followed by the theory. There was also indicating that the Reaction Volume greater as the coagulin Pressure was increased.

(3) At high Frequencies, the operation between theory and experiment indeed are very similar. It is expected that the operation investigated should be limited to the range of Reynolds Numbers 10^5 and 10^6.

(4) Though the above and applicable measurements seemed reasonably well within experimental error, the correlations was not satisfactorily given in determine a value of the Bundling or difference available at the assembly.

IX. LITERATURE CITED

1. Campbell, D. C. and Stelson, P. H. Relaxation times of a subcritical reactor by pulsed neutron techniques. American Physical Society Bull. 1: 183. 1956.

2. Glasstone, S. and Edlund, M. S. Elements of nuclear reactor theory. Princeton, N. J., D. Van Nostrand Co., Inc. 1952.

3. Murray, R. L. Nuclear reactor physics. Englewood, N. J., Prentice-Hall, Inc. 1957.

4. Naievski, V. and Horowitz, J. Determination of the mean transfer free path of thermal neutrons by measurement of the complex diffusion length. [1st.] International Conference on the Peaceful Uses of Atomic Energy, Geneva, 1955. Proceedings 5: 42-51. 1956.

5. Sjöstrand, N. G. Measurements on a subcritical reactor with a pulsed neutron source. [1st.] International Conference on the Peaceful Uses of Atomic Energy, Geneva, 1955. Proceedings 5: 52-54. 1956.

6. Uhrig, R. E. Operating characteristics of a graphite moderated subcritical assembly. Nuclear Science and Engineering. 5: 120-126. 1959.

7. _____. Material buckling measurements in a subcritical assembly. American Nuclear Society Transactions. 2: 61-62. 1959.

8. Weinberg, A. M. and Schweinler, H. C. Theory of oscillating absorber in a chain reactor. Physical Review. 74: 851-863. 1948.

9. _____ and Wigner, E. P. Physical theory of neutron chain reactors. Chicago, Ill., University of Chicago Press. 1958.

10. Worthing, A. G. and Geffner, J. Treatment of experimental data. New York, N. Y., John Wiley and Sons, Inc. 1943.

X. ACKNOWLEDGMENTS

The author is deeply indebted to Dr. Robert E. Uhrig who suggested this original topic, introduced him to the subject and aided him unsparingly during the course of the experiment.

The wise advice and assistance of Dr. Glenn Murphy throughout the past year is gratefully acknowledged.

This culminates three years of advanced education under the auspices of the United States Navy. It is with a sincere sense of gratitude that I acknowledge the opportunities offered to me by this advanced education, and a hope that I will be able to repay that trust.

XI. APPENDIX A: TABLES OF DATA

Table 1. Data at 506 rpm

Channel	Duration	N_B	N_D	N_A	N_C
1a	4	42260	39698	42258	39114
		42221	39742	42527	39299
		42174	39301	42772	39284
1b	4	97683	93187	100509	89989
		97415	91408	99499	89832
		97678	91696	99676	89703
			92073	99390	90001
1c	4	121976	120465	129595	113518
		122188	119310	128795	111625
		121565	120030	128342	112485
		121616	119548	129455	112315
		122234	120184	129096	112410
2a	14	74344	71637	75176	70770
2b	7	83591	81784	86568	79529
		83796	82860	85378	79144
		84213	80788	85389	79135
		83820	81180	86651	80448
		84195	81929	85697	79600
		83545	81751	85954	79494
		83412	81291	85806	79338
		84438	81700		
2c	7	103237	100810	105859	98334

Table 1. (Continued)

Channel	Duration	N_B	N_D	N_A	N_C
		102137	101062	105381	97297
		89096	88288	93894	87029
2d	10	115763	115544	119386	111309
2e	14	68072	68595	71268	66169
3b	20	108821	105493	110107	102173
		103354	100423	105779	98331
3c	15	98035	96718	100987	94308
		98276	96022	100301	94368
		99487	97709	102708	95281
3d	20	107331	105911	110569	102770
4a	45	49063	47750	50589	47291
4b	35	83313	80766	84781	79662
		83020	81375	84709	79700
4c	35	100700	97974	102881	96271
		101205	98080	102577	96695
		100662	98509	102662	96304
		100331	98553	102784	97015
4d	20	47932	46379	48668	45721
4e	45	50016	48945	50692	48066
5b	80	83045	80281	83728	78745
5c	80	100109	98614	102070	96191

Table 1. (Continued)

35	14	1,211,952	1,211,952	1,211,952	1,211,952
36	15	1,211,952	1,211,952	1,211,952	1,211,952
37	16	1,211,952	1,211,952	1,211,952	1,211,952
38	17	1,211,952	1,211,952	1,211,952	1,211,952
39	18	1,211,952	1,211,952	1,211,952	1,211,952
40	19	1,211,952	1,211,952	1,211,952	1,211,952
41	20	1,211,952	1,211,952	1,211,952	1,211,952
42	21	1,211,952	1,211,952	1,211,952	1,211,952
43	22	1,211,952	1,211,952	1,211,952	1,211,952
44	23	1,211,952	1,211,952	1,211,952	1,211,952
45	24	1,211,952	1,211,952	1,211,952	1,211,952
46	25	1,211,952	1,211,952	1,211,952	1,211,952
47	26	1,211,952	1,211,952	1,211,952	1,211,952
48	27	1,211,952	1,211,952	1,211,952	1,211,952
49	28	1,211,952	1,211,952	1,211,952	1,211,952
50	29	1,211,952	1,211,952	1,211,952	1,211,952

Table 2. Data at 1308 rpm

Channel	Duration	N_B	N_D	N_A	N_C
1c	4	120850	114639	126617	107860
		121246	114101	126641	108097
		170616	115112	126369	108143
2c	7	101812	95960	103664	94050
		101640	95699	103407	94407
3c	15	97215	91338	98715	90269
4c	35	98915	91486	100016	91654

XII. APPENDIX B: PHASE ANGLE AND AMPLITUDE TABULATION

Table 3. Phase angle and amplitude in various channels

Channel		θ	R_w
1a	506	38° 5' ± 3°53'	1,658 ± 112
1b		29°06' ± 2°13'	4,430 ± 171
1c		6°54' ± 1°41'	6,550 ± 192
2a		31°34' ± 4°14'	581 ± 43
2b		19°07' ± 3°26'	1,519 ± 91
2c		10°52' ± 3°14'	1,711 ± 99
2d		1°33' ± 3°25'	1,269 ± 76
2e		-5°53' ± 4°08'	574 ± 42
3b		22°08' ± 3°10'	651 ± 36
3c		17°05' ± 3°32'	752 ± 46
3d		10°19' ± 3°20'	623 ± 36
4a		21°42' ± 5°02'	124 ± 11
4b		22°01' ± 4°14'	246 ± 18
4c		21°41' ± 3°51'	296 ± 20
4d		27°46' ± 5°16'	262 ± 24
4e		22°08' ± 6°20'	99 ± 11
5b		29°01' ± 4°04'	112 ± 8
5c		14°15' ± 4°10'	119 ± 9
1c	1308	18°46' ± 1°26'	7,670 ± 192
2c	1308	32°22' ± 2°19'	2,467 ± 100

Table 3. (Continued)

Channel		θ	R_w
3c	1308	34°50' ± 2°26'	1,077 ± 46
4c	1308	41°37' ± 2°15'	502 ± 20

XIII. APPENDIX C: EVALUATION OF NEUTRON FLUX COEFFICIENTS

The flux at any point in the assembly was given in Part IV as

$$\phi = \sum_{m=1}^{\infty} \sum_{n=1}^{\infty} \cos \frac{m\pi x}{a} \cos \frac{n\pi y}{b} \left[A_{mn} e^{-\gamma_{mn} z} + C_{mn} e^{i\omega t - \rho_{mn} z} \right] \tag{25}$$

In order to determine the relative importance of the various lower modes, it is necessary to evaluate the constants A_{mn} and C_{mn}.

The source is considered as a point source at the origin emitting neutrons at a rate $S_t = S_o + Se^{i\omega t}$ neutrons per second. A source of this kind may be written as $S\,\delta(x,y)$ at $z = 0$, where $\delta(x,y)$ is the Dirac delta function, which is defined to be zero everywhere except at $x = y = 0$, where it has a value such that

$$\int_{-\infty}^{\infty} \int_{-\infty}^{\infty} \delta(x,y)\, dx\, dy = 1 \tag{C1}$$

It is to be seen that as a consequence of this definition of the delta function

$$\int_{-\infty}^{\infty} f(x)\, \delta(x)\, dx = f(0) \tag{C2}$$

or in other words, the value of any integral containing the delta function is merely the value of the function being integrated, evaluated at zero. For the point source under

consideration, the source term may be written

$$S_t = S_t \int_{-\infty}^{\infty} \int_{-\infty}^{\infty} \delta(x,y)\, dx\, dy \qquad (C3)$$

$$= \int_{-\infty}^{\infty} \int_{-\infty}^{\infty} (S_o + Se^{i\omega t})\, \delta(x,y)\, dx\, dy$$

In order to determine A_{mn} and C_{mn}, expand the source in a series of orthogonal functions that satisfy the boundary condition that it is $S_t\, \delta(x,y)$ at $z = 0$

$$(S_o + Se^{i\omega t})\, \delta(x,y) = \sum_{m=1}^{\infty} \sum_{n=1}^{\infty} (S_{o_{mn}} + S_{mn}e^{i\omega t})$$

$$\cos \frac{m\pi x}{a} \cos \frac{n\pi y}{b} \qquad (C4)$$

where the values $S_{o_{mn}}$ and $S_{mn}e^{i\omega t}$ are coefficients related to the source strength.

To determine the $S_{o_{mn}}$ and S_{mn} terms, each side of Equation C4 is multiplied by $\cos \frac{k\pi x}{a} \cos \frac{l\pi y}{b}$ and integrated over the range $-\frac{1}{2}a \leq x \leq \frac{1}{2}a$ and $-\frac{1}{2}b \leq y \leq \frac{1}{2}b$. These limits of integration may be used because values of the function S_t outside this range are zero, and of course integrate to zero.

Since the functions are orthogonal in the intervals investigated, all terms having $m \neq k$ and $n \neq l$ will vanish. Equation C4 becomes

$$(S_o + Se^{i\omega t}) \int_{-\frac{a}{2}}^{\frac{a}{2}} \int_{-\frac{b}{2}}^{\frac{b}{2}} \delta(x,y) \cos \frac{m\pi x}{a} \cos \frac{n\pi y}{b}$$

$$= (S_{o_{mn}} - S_{mn}e^{i\omega t}) \int_{-\frac{a}{2}}^{\frac{a}{2}} \cos^2 \frac{m\pi x}{a}\, dx \int_{-\frac{b}{2}}^{\frac{b}{2}} \cos^2 \frac{n\pi y}{b}\, dy \qquad (C5)$$

The integral on the left is, as a consequence of Equation C2

$$(S_o + Se^{i\omega t}) \cos \frac{m\pi 0}{a} \cos \frac{n\pi 0}{b} = S_o + Se^{i\omega t} \qquad (C6)$$

The two integrals on the right reduce to $\frac{1}{2}a$ and $\frac{1}{2}b$ respectively. Hence, Equation C5 reduces to

$$\frac{4(S_o + Se^{i\omega t})}{ab} = S_{o_{mn}} + S_{mn}e^{i\omega t} \qquad (C7)$$

The real and imaginary parts on both sides of this equation are equal. Therefore

$$S_{o_{mn}} = \frac{4S_o}{ab} \qquad (C8)$$

$$S_{mn} = \frac{4S}{ab} \qquad (C9)$$

The source condition to be satisfied is that the number of neutrons flowing out of the plane z = 0 per $cm.^2$ per second in each mode must be equal to the number produced in that mode by the source. If the assumption is made that the current density in the mn mode in the z direction is equal to one half the neutrons produced by the source in that mode, the current density is equal to one half of the value of the source contribution of Equation C4, or

$$J_{mn} = \tfrac{1}{2}(S_{o_{mn}} + S_{mn}e^{i\omega t}) \cos \frac{m\pi x}{a} \cos \frac{n\pi y}{b} \qquad (C10)$$

Substituting the values of $S_{o_{mn}}$ and S_{mn} from Equations C8 and C9

$$J_{mn} = \frac{1}{2}\left[\frac{4S_o}{ab} + \frac{4S_e i\omega t}{ab}\right] \cos\frac{m\pi x}{a} \cos\frac{n\pi y}{b} \qquad (C11)$$

The current density is related to flux by

$$J_{mn} = -D\left(\frac{\partial\phi_{mn}}{\partial z}\right)_o \qquad (C12)$$

$$J_{mn} = D\, A_{mn}\, \gamma_{mn} \cos\frac{n\pi x}{a} \cos\frac{n\pi y}{b}$$

$$+ D\, C_{mn}\, \rho_{mn} \cos\frac{m\pi x}{a} \cos\frac{n\pi y}{b}\, e^{i\omega t} \qquad (C13)$$

Equating Equations C11 and C13

$$A_{mn} = \frac{2\, S_o}{a\, b\, D\, \gamma_{mn}} \qquad (C14)$$

$$C_{mn} = \frac{2\, S}{a\, b\, D\, \rho_{mn}} \qquad (C15)$$

The complete equation for the flux is

$$\phi = \sum_{m=1}^{\infty}\sum_{n=1}^{\infty} \frac{2\, S_o}{a\, b\, D\, \gamma_{mn}} \cos\frac{m\pi x}{a} \cos\frac{n\pi y}{b}\, e^{-\gamma_{mn} z}$$

$$+ \frac{2\, S}{a\, b\, D\, \rho_{mn}} \cos\frac{m\pi x}{a} \cos\frac{n\pi y}{b}\, e^{-\rho_{mn} z}\, e^{i\omega t} \qquad (C16)$$

While it is not possible in this experiment to solve for S_o and S directly, the ratio of the two quantities can be determined. If points on the z axis only are investigated, and if the following substitutions are performed

$$A_c = \frac{2\, S_o}{a\, b\, D}$$

$$A_1 = \frac{2\,S}{a\,b\,D}$$

Equation C16 reduces to

$$\phi = \sum_{m=1}^{\infty} \sum_{n=1}^{\infty} \frac{A_o}{\gamma_{mn}} e^{-\gamma_{mn} z} + \frac{A_1}{\rho_{mn}} e^{-\rho_{mn} z}\, e^{i\omega t} \qquad (C17)$$

In order to investigate the effect of the various higher modes, the flux contributions of the lowest four modes was determined, and their cumulative totals plotted in Figure 19. The ordinate is plotted in units proportional to the source strength. For the angular velocity investigated, 506 rpm, γ_{mn} and ρ_{mn} are so close in value that the ordinate can be considered either as units of A_o or A_1 of Equation C17.

To determine the shape of the emitted wave, static counts were taken at each 10° of drum rotation, yielding the curves of Figure 18. The amplitude of the sine wave in this figure is proportional to either S or the defined quantity A_1, while the steady state or average count is proportional to the values S_o or A_o. For channel 1c the ratio of these amplitudes was

$$\frac{S}{S_o} \doteq 0.11 \qquad (C18)$$

This ratio decreases with distance from the source. Thus, the value given in Equation C18 is to be considered as an approximation only of the wave amplitude to steady state amplitude, and it is applicable only to the 12" level.

$$\lambda_f = \frac{\omega_f}{k + k_f}$$

Equation (23) reduces to

$$\lambda = \frac{\omega_{ext}}{k_{ext}} e^{-i\omega_{ext}t} \; ; \; \frac{k_f}{k_{ext}} e^{-i\omega_f t} e^{ikx} \qquad (27)$$

In order to investigate the effect of the various slider modes, the first derivatives of the output flow modes are determined, and shown graphically in Figure 28. The ordinate is scaled in units proportional to the source strength. For the source velocity investigated, ω_{ext} and ω_f can be given in value that the ordinate can be considered either as units of k_f or ω_f of Equation (27).

In examining the shape of the modified wavy slider modes were taken at each $\frac{1}{4}$ of their relative wavelengths of Figure 11. The amplitude of the wave in this figure is proportional to either a or the initial viscosity k_f, while the steady state or resting mode is proportional to the volume σ or $\frac{1}{k_f}$. The inverse of the ratio of these amplitudes are

$$\frac{\sigma}{a} \qquad (28)$$

This ratio increasing with distance from the source. Thus, the wavy slider shown in Figure 11a is to be considered as an approximation only of the wavy slider, since a finite amplitude, and it is applicable only to the 12" model.

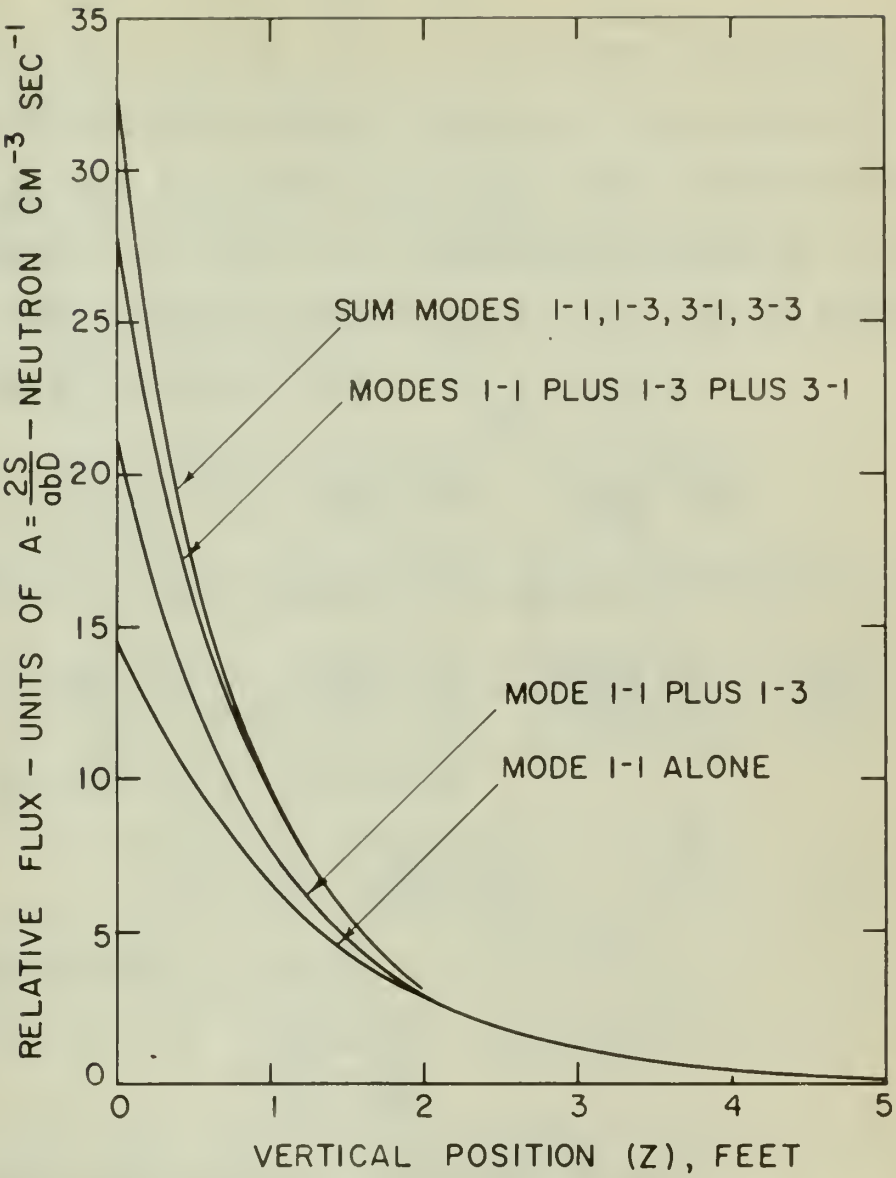

Figure 19. Flux contributions of various modes

XIV. APPENDIX D: CALCULATION OF STANDARD DEVIATION

In order to determine the precision of the data taken, evaluation of the standard deviation in each value of phase angle and wave amplitude were made. The generalized formula for standard deviation of a dependent function u, in terms of the independent variables x_1, x_2, x_3, etc. is given in Worthing and Geffner (10).

$$\sigma_u^2 = \left[\frac{\partial u}{\partial x_1}\right]^2 \sigma_{x_1}^2 + \left[\frac{\partial u}{\partial x_2}\right]^2 \sigma_{x_2}^2 + \left[\frac{\partial u}{\partial x_3}\right]^2 \sigma_{x_3}^2 + \ldots \qquad (D1)$$

If this generalized equation is applied to Equation 53

$$\sigma_\theta^2 = \left[\frac{\partial \theta}{\partial N_A}\right]^2 \sigma_{N_A}^2 + \left[\frac{\partial \theta}{\partial N_B}\right]^2 \sigma_{N_B}^2 + \left[\frac{\partial \theta}{\partial N_C}\right]^2 \sigma_{N_C}^2 + \left[\frac{\partial \theta}{\partial N_D}\right]^2 \sigma_{N_D}^2 \qquad (D2)$$

where Equation 53 is written as

$$\theta = \tan^{-1} \frac{N_B - N_D}{N_A - N_C} \qquad (53)$$

For convenience, we define

$$\gamma \equiv \frac{N_B - N_D}{N_A - N_C} \qquad (D3)$$

The partial derivatives of Equation 53 are

$$\frac{\partial \theta}{\partial N_A} = \frac{-\gamma}{(1+\gamma^2)(N_A - N_C)} \qquad (D4)$$

$$\frac{\partial \theta}{\partial N_B} = \frac{1}{(1+\gamma^2)(N_A - N_C)} \qquad (D5)$$

XIV. APPENDIX B: CALCULATION OF STANDARD DEVIATIONS

In order to determine the precision of the data derived from the standard deviations of the standard functions in each value of phase angle and wave number/light wave number. The procedure involves the standard deviation of a dependent function y, is found at the independent variables x_1, x_2, x_3 etc. It gives is applied and derived thus:-

$$\sigma_y^2 = \left[\frac{\partial y}{\partial x_1}\right]^2 \sigma_{x_1}^2 + \left[\frac{\partial y}{\partial x_2}\right]^2 \sigma_{x_2}^2 + \left[\frac{\partial y}{\partial x_3}\right]^2 \sigma_{x_3}^2 + \cdots \qquad (1)$$

If this generalized equation is applied to equation 2)

$$\sigma_\varepsilon^2 = \left[\frac{\partial \varepsilon}{\partial E}\right]^2 \sigma_E^2 + \left[\frac{\partial \varepsilon}{\partial \gamma}\right]^2 \sigma_\gamma^2 + \left[\frac{\partial \varepsilon}{\partial \alpha}\right]^2 \sigma_\alpha^2 + \left[\frac{\partial \varepsilon}{\partial \beta}\right]^2 \sigma_\beta^2 \qquad (2)$$

where equation 2) is written as

$$\varepsilon = \tan^{-1} \frac{\gamma - \alpha}{\beta - \alpha} \qquad (3)$$

For convenience, we define

$$\gamma = \frac{\beta - \alpha}{\varepsilon} \qquad (4)$$

The partial derivatives of equation 3) are

$$\frac{\partial \varepsilon}{\partial \gamma} = \frac{1}{(\beta - \alpha)(1 + \gamma^2)} \qquad (5)$$

$$\frac{\partial \varepsilon}{\partial \beta} = \frac{-(\gamma - \alpha)}{(\beta - \alpha)^2 (1 + \gamma^2)} \qquad (6)$$

$$\frac{\partial \theta}{\partial N_C} = \frac{\tau}{(1 + \tau^2)(N_A - N_C)} \tag{D6}$$

$$\frac{\partial \theta}{\partial N_D} = \frac{-1}{(1 + \tau^2)(N_A - N_C)} \tag{D7}$$

The individual standard deviations are

$$\sigma_{N_A} = (N_A)^{\frac{1}{2}} \tag{D8}$$

$$\sigma_{N_B} = (N_B)^{\frac{1}{2}} \qquad \sigma_{N_D} = (N_D)^{\frac{1}{2}}$$

$$\sigma_{N_C} = (N_C)^{\frac{1}{2}}$$

Substitution of the given values in the generalized formula gives

$$\sigma_\theta^2 = \frac{\tau^2 N_A}{(1 + \tau^2)^2 (N_A - N_C)^2} + \frac{N_B}{(1 + \tau^2)^2 (N_A - N_C)^2}$$

$$+ \frac{\tau^2 N_C}{(1 + \tau^2)^2 (N_A - N_C)^2} + \frac{N_D}{(1 + \tau^2)^2 (N_A - N_C)^2} \tag{D9}$$

As the sum of $(N_A + N_C)$ is equal to both the total count and the sum $(N_B + N_D)$, Equation D9 can be simplified to

$$\sigma_\theta^2 = \frac{N_A + N_C}{(N_A - N_C)^2 + (N_B - N_D)^2} \tag{D10}$$

In a similar manner, the standard deviation in the sine amplitude can be determined. The generalized equation is

$$\sigma_{R_W}^2 = \left[\frac{\partial R_W}{\partial N_A}\right]^2 \sigma_{N_A}^2 + \left[\frac{\partial R_W}{\partial N_B}\right]^2 \sigma_{N_B}^2 + \left[\frac{\partial R_W}{\partial N_C}\right]^2 \sigma_{N_C}^2 + \left[\frac{\partial R_W}{\partial N_D}\right]^2 \sigma_{N_D}^2 \tag{D11}$$

From Equation 54

$$\frac{\partial \mathcal{L}}{\partial \theta} = \frac{(1+\lambda_2)(\mathcal{L}^1 - \mathcal{L}^2)}{2} \tag{309}$$

$$\frac{\partial \mathcal{L}}{\partial \theta} = \frac{(1+\lambda_2)(\mathcal{L}^1 - \mathcal{L}^2)}{1} \tag{310}$$

The boundary equality conditions are

$$\begin{aligned} Q^1 &= (\mathcal{L}^1)_1 \\ Q^{\frac{1}{2}} &= (\mathcal{L}^{\frac{1}{2}})_1 \qquad Q^{\frac{1}{2}} = (\mathcal{L}^{\frac{1}{2}})_2 \\ Q^0 &= (\mathcal{L}^0)_1 \end{aligned} \tag{311}$$

Substitution of the above values in the quadratic formula

gives

$$Q^0_2 = \frac{(1+\lambda_2)_1(\mathcal{L}^1 - \mathcal{L}^2)_2}{\lambda_2 \theta^2} + \frac{(1+\lambda_2)_1(\mathcal{L}^1 - \mathcal{L}^2)_2}{\theta^2}$$

$$+ \frac{(1+\lambda_2)_1(\mathcal{L}^1 - \mathcal{L}^2)_2}{\lambda_2 \theta^2} + \frac{(1+\lambda_2)_1(\mathcal{L}^1 - \mathcal{L}^2)_2}{\theta^2} \tag{312}$$

As the sum of $(\mathcal{L}^1 - \mathcal{L}^2)$ is equal to both the first second and the sum $(\mathcal{L}^1 - \mathcal{L}^2)$, Equation 31 can be simplified to

$$Q^0_2 = \frac{(\mathcal{L}^1 - \mathcal{L}^2)_1 - (\mathcal{L}^1 - \mathcal{L}^2)_2}{\theta^2} \tag{313}$$

In a similar manner, the boundary situation in the plus equality can be determined. The quadratic equation is

$$Q^{\frac{1}{2}}_2 + \left[\frac{\partial \mathcal{L}}{\partial \theta}\right]_1 Q^{\frac{1}{2}}_2 + \left[\frac{\partial \mathcal{L}}{\partial \theta}\right]_2 Q^{\frac{1}{2}}_2 - \left[\frac{\partial \mathcal{L}}{\partial \theta}\right]_2 Q^{\frac{1}{2}}_2 - \left[\frac{\partial \mathcal{L}}{\partial \theta}\right]_2 Q^{\frac{1}{2}}_2 \tag{314}$$

Upon inversion it

$$R_w = \frac{\pi}{2\ nT'} \left[(N_B - N_D)^2 + (N_A - N_C)^2 \right]^{\frac{1}{2}} \tag{54}$$

If the substitution

$$\rho^2 = (N_B - N_D)^2 + (N_A - N_C)^2 \tag{D12}$$

is used, the partial derivatives are found to be

$$\begin{aligned}
\frac{\partial R_w}{\partial N_A} &= \frac{\pi}{2\ nT'} \frac{(N_A - N_C)}{\rho} \\
\frac{\partial R_w}{\partial N_B} &= \frac{\pi}{2\ nT'} \frac{(N_B - N_D)}{\rho} \\
\frac{\partial R_w}{\partial N_C} &= \frac{-\pi}{2\ nT'} \frac{(N_A - N_C)}{\rho} \\
\frac{\partial R_w}{\partial N_D} &= \frac{-\pi}{2\ nT'} \frac{(N_B - N_D)}{\rho}
\end{aligned} \tag{D13}$$

Substituting in Equation D11

$$\begin{aligned}
\sigma^2_{R_w} = {} & N_A \left[\frac{\pi}{2\ nT'}\right]^2 \frac{(N_A - N_C)^2}{\rho^2} + N_B \left[\frac{\pi}{2\ nT'}\right]^2 \frac{(N_B - N_D)^2}{\rho^2} \\
& + N_C \left[\frac{\pi}{2\ nT'}\right]^2 \frac{(N_A - N_C)^2}{\rho^2} + N_D \left[\frac{\pi}{2\ nT'}\right]^2 \frac{(N_B - N_D)^2}{\rho^2}
\end{aligned} \tag{D14}$$

Upon simplifying and substituting, the standard deviation in the sine amplitude is found to be

$$\sigma_{R_w} = \frac{\pi}{2\ nT'} (N_A + N_C)^{\frac{1}{2}} \tag{D15}$$

thesH9575
Characteristics of neutron waves in a su
3 2768 002 13292 0
DUDLEY KNOX LIBRARY